Deciphering tectonic, eustatic and surface controls on the 20 Ma-old Burdigalian transgression recorded in the Upper Marine Molasse in Switzerland

Philippos Garefalakis[1], Fritz Schlunegger[1]

[1]Institute of Geological Sciences, University of Bern, Bern, CH-3012, Switzerland

Correspondence to: Philippos Garefalakis (philippos.garefalakis@geo.unibe.ch)

Abstract

The stratigraphic architecture of the Swiss Molasse basin reveals crucial information about the basin's geometry, its evolution and the processes leading to the deposition of the clastic material. Nevertheless, the formation of the Upper Marine Molasse (OMM) and the controls on the related Burdigalian transgression are not fully understood yet. During these times, from c. 20 to 17 Ma, the Swiss Molasse basin was partly flooded by a peripheral shallow marine sea, striking SW – NE. We proceeded through detailed sedimentological and stratigraphic examinations of several sites across the entire Swiss Molasse basin in order to deconvolve the stratigraphic signals related surface and tectonic controls. Surface-related signals include stratigraphic responses to changes in eustatic sea level and sediment fluxes, while the focus on crustal-scale processes lies on the uplift of the Aar-massif at c. 20 Ma.

Field examinations show that the evolution of the Burdigalian seaway was characterized by (i) shifts in the depositional settings, (ii) changes in discharge directions, (iii) deepening and widening of the basin, and (iv) phases of erosion and non-deposition. We relate these changes in the stratigraphic record to a combination of surface and tectonic controls at various scales. In particular, roll-back subduction of the European mantle lithosphere, delamination of crustal material and the associated rise of the *Aar-massif* most likely explain the widening of the basin particularly at distal sites. In addition, the uplift of the *Aar-massif* was likely to have shifted the patterns of surface loads. These mechanisms could have caused a flexural adjustment of the foreland plate underneath the Molasse basin, which we use as mechanism to explain the establishment of distinct depositional environments and particularly the formation of subtidal-shoals where a lateral bulge is expected. In the Alpine hinterland, these processes occurred simultaneously with a period of fast tectonic exhumation accomplished through slip along the *Simplon* detachment fault, with the consequence that sediment flux to the basin decreased. It is possible that this reduction in sediment supply contributed to the establishment of marine conditions in the Swiss Molasse basin and thus amplified the effect related to the tectonically controlled widening of the basin. Because of the formation of shallow marine conditions, subtle changes in the eustatic sea level contributed to the occurrence several hiatus that chronicle periods of erosion and non-sedimentation. While these mechanisms are capable of explaining the establishment of the Burdigalian

seaway and the formation of distinct sedimentological niches in the Swiss Molasse basin, the drainage reversal during OMM-times possibly requires a change in the tectonic processes at the slab scale.

We conclude that sedimentological records can be used to decipher surface controls and lithospheric-scale processes in orogens from the stratigraphic record, provided that a detailed sedimentological and chronological database is available.

1 Introduction

Foreland basins and their deposits have often been used for exploring the tectonic evolution of their hinterlands, mainly because these basins are mechanically coupled with the adjacent mountain belts (Beaumont, 1981; Jordan, 1981; DeCelles, 2004). The formation of the basins occurs through the flexural bending of the underlying lithosphere, which creates accommodation space (DeCelles and Giles, 1996; Allen and Allen, 2005). The shape of the foreland trough depends on the mechanical properties of the foreland plate (Sinclair et al., 1991; Flemings and Jordan, 1990; Jordan and Flemings, 1991), the volume and thickness of the sedimentary fill (Flemings and Jordan, 1990; Jordan and Flemings, 1991) and particularly on the tectonic and geodynamic processes leading to changes in the plate loading (Beaumont, 1981; Allen et al., 1991; DeCelles and Gilles, 1996). In this context, the sedimentary fill, which commonly record Flysch and Molasse phases (Sinclair and Allen, 1992), reveal crucial information about the basin's geometry and evolution. Within this context, the North Alpine Foreland Basin (NAFB), or Molasse basin (Fig. 1), is probably one of the best-studied foreland basins and has been examined in detail over the past decades (e.g. Matter et al., 1980; Homewood and Allen, 1981; Allen, 1984; Keller, 1989; Schlunegger et al., 1996, 1997; Kempf et al., 1999; Kuhlemann and Kempf, 2002). The approximately 700 km long ENE – WSW striking basin stretches from France to Austria, where it broadens to a maximum width of c. 150 km (Pfiffner, 1986; Fig. 1). The NAFB is limited to the south by the Alpine fold-and thrust belt, and to the north by the Jura Mountains and the Black-Forest- and Bohemian-massifs (Homewood et al., 1986).

Here, we centre our work on the central part of the NAFB, commonly referred to as the Swiss Molasse basin (Fig. 1), which stretches from Lake Geneva to Lake Constance over a total length of c. 270 km and a maximum width of c. 80 km (Fig. 2). We particularly focus on the c. 20 Ma-old Burdigalian transgression and pay special attention on establishing the link between the sedimentary processes recorded by the Upper Marine Molasse (OMM) deposits and the contemporaneous geometrical changes of the basin. The extension and dimension of the Burdigalian seaway are well known, and several authors (e.g. Allen, 1984; Allen et al. 1985; Homewood et al. 1986; Matter, 1964; Burbank et al., 1992; Kempf, 1998; Kempf et al., 1997; Keller, 1989; Strunck and Matter, 2002; Schlunegger, 1996, 1997; Kuhlemann and Kempf, 2002) examined paleo-discharge directions, sedimentary thicknesses, and depositional environments of the OMM. Furthermore, these authors were also discussing possible controls leading to the marine ingression. Despite these efforts, the controls on the Burdigalian transgression in this basin are not fully understood yet. Previous authors (e.g. Allen et al., 1985; Homewood et al., 1986; Keller, 1989; Strunck and Matter, 2002) proposed a combination of a reduced sediment flux and a rise in global sea level as possible mechanisms. However, the Burdigalian was also the time when the external massifs in the Alps

experienced a period of flexural uplift (Boston et al., 2017; Herwegh et al., 2017), which could have contributed to the flexural downwarping of the foreland plate and thus to the transgression of the peripheral sea (Sinclair et al., 1991). It appears that these diverging views on the driving forces are mainly due to the rather regional focus of the aforementioned studies. In particular, previous authors mainly focused either on the western (e.g. Strunck and Matter, 2001), the central (e.g. Sinclair et al., 1991; Schlunegger et al., 1996; 1997) or the eastern part (e.g. Keller, 1989; Kempf et al., 1999) of the Swiss Molasse basin. Here, we analysed outcrops and sections along the entire Swiss basin situated at both proximal and distal positions in relation to the Alpine front (Fig. 2) with a particular focus on the 20 Ma-old Burdigalian transgression. We aim to explain, through a sedimentological and stratigraphic approach at the basin scale, the influence of possible controls on this transgression including: (i) an eustatic rise in sea level, (ii) a reduction in sediment flux or (iii) an increase in tectonically controlled accommodation space.

2 Setting

2.1 The Swiss Molasse Basin and the Central European Alps

The deposits of the Swiss Molasse basin record two large-scale transgressive-regressive mega-sequences deposited between c. 32 and 10 – 5 Ma (e.g. Sinclair, 1997; Kempf et al., 1997, 1998; Kuhlemann and Kempf, 2002; Cederbom et al., 2004; 2011). These two shallowing-up mega-sequences consist of four lithostratigraphic groups, for which we employ the common German abbreviations in this work (Matter et al., 1980). Prior to the first mega-cycle, from approximately 35 Ma to 32 Ma, the North Helvetic Flysch (NHF, early Oligocene) was deposited during the underfilled Flysch basin stage (Sinclair and Allen, 1992). The Flysch period was characterized by a deep marine trench close to the evolving Alps where turbidity currents resulted in the accumulation of mud- and sandstone on submarine fans (Allen et al. 1991; Lu et al., 2018). This stage was followed by a regressive sequence, when the initial rise of the Alps c. 32 – 30 Ma ago (e.g., Garefalakis and Schlunegger, 2018) was associated with fast erosion and large sediment fluxes to the Molasse basin (Sinclair, 1997). This resulted in the deposition of the Lower Marine Molasse Group (UMM, Rupelian), consisting of shallow-marine mud- and sandstones (Diem, 1986) and recording the end of the underfilled stage. The first mega-sequence was finally terminated by the deposition of conglomerates, sandstones and mudstones of the terrestrial (overfilled basin) Lower Freshwater Molasse Group (USM; Platt and Keller, 1992) between the early Oligocene and the early Miocene (Rupelian to Aquitanian). The second transgressive-regressive cycle started with the deposition of shallow-marine sand- and mudstones of the Upper Marine Molasse Group (OMM) around 20 Ma (Burdigalian). This second mega-cycle ended with conglomerates and sandstones of the regressive, terrestrial Upper Freshwater Molasse Group (OSM) during late Burdigalian to late Serravallian times. Sedimentation in the Molasse basin continued up to c. 10 – 5 Ma, when a phase of uplift resulted in the erosion and the recycling of previously deposited Molasse deposits (Mazurek et al., 2006: Cederbom et al., 2004; 2011).

The basin is bordered to the south by the doubly vergent Alpine orogen (Fig. 1b). It comprises a nappe stack with a crystalline core that is exposed in the Lepontine dome and the external massifs (e.g. Aar-massif; Spicher, 1980). The orogen

is underlain by a thick crustal root made up of a stack of lower crustal material derived from the European continental plate (Fry et al., 2010). At deeper levels, the c. 160 km-long (Lippitsch et al., 2003) slab of the European mantle lithosphere bends the foreland plate towards the south-east, resulting in a downwarping of the European plate (Fig. 1b). The large-scale deflection of the plate and the formation of accommodation space in the Molasse basin is thus the consequence of this bending (Schlunegger and Kissling, 2015). In addition, the modern topography is formed in response to the isostatic equilibrium between the buoyancy of the crustal root and the vertically directed slab-load forces (Kissling, 1993; Kissling and Schlunegger, 2018).

The Alpine architecture is the consequence of the Late Cretaceous to present continent-continent collision between the European and Adriatic plates, which resulted in the build up of the Alpine edifice (Schmid et al., 1996). At 20 Ma, the phase of nappe stacking was superseded by a period of vertical extrusion of the Lepontine dome (Hurford, 1986) and the Aar-massif (Herwegh et al., 2017). This was also the time, when the slip along the Simplon detachment fault occurred at the fastest rates, resulting in the fast exhumation of deeper crustal levels to the surface (Mancktelow, 1985; Mancktelow and Grasemann, 1997; Boston et al., 2017).

2.2 The Upper Marine Molasse

The Upper Marine Molasse (OMM) deposits, which are the focus of this paper, mainly comprise a suite of sandstones and mudstone interbeds. In the central basin, these sediments were deposited in a shallow marine, c. 70 – 80 km-wide seaway during Burdigalian times between c. 20 – 17 Ma (Allen and Homewood, 1984; Allen et al., 1985; Keller, 1989). At the proximal basin border, the OMM-successions are up to 900 m thick and thin to a few tens of meters towards the distal basin margin. Thick conglomerate packages situated at the Alpine thrust front (*Napf* conglomerates) separated the basin into an eastern and western segment (Fig. 3). East of the *Napf* conglomerates, in the following denoted as the *Napf-units* (Matter, 1964), the OMM has been grouped into the *Lucerne-* and the *St. Gallen-Formations* (Keller, 1989), which are separated by a m-thick paleosoil. For simplicity purposes, we will refer to these units as the OMM-I (*Lucerne-Fm)* and the OMM-II (*St. Gallen-Fm)*, respectively. In the distal basin, also east of the *Napf-units*, the OMM-I deposits comprise a suite of sandstone beds at the base, followed by a succession of shelly-sandstones ("Muschelsandstein"; Jost et al., 2016) at the top. The overlying OMM-II comprises conglomerates, sandstones and mudstones (Jost et al., 2016). West of the *Napf-units*, the OMM has been grouped in three units (Fig. 3), which are from the base to the top: the *Sense-beds* (suite of sandstones with mudstone interbeds), *the Kalchstätten-Formation* (alternation of sandstones and mudstones) and *the Guggershorn-Formation* (succession of conglomerates with sandstone interbeds) (Strunck and Matter, 2002). As will be shown later, the *Sense-beds* and *Kalchstätten-Fm* correspond to the OMM-I, while the *Guggershorn-Fm* is a time-equivalent of the OMM-II. Similar to the east, the western distal basin is made up of sandstones at the base, and "Muschelsandstein" deposits at the top. As outlined above, the Pliocene phase of uplift and erosion (Cederbom et al., 2004; 2011) resulted in the current exposure pattern where OMM deposits are only fragmentarily preserved in the west (Fig. 2).

3 Methods

3.1 Sedimentological investigations and study sites

We applied state-of-the-art sedimentological techniques to examine different sections through time. The research sites are located at both proximal and distal positions within the basin. We explored these sections for environmental conditions, the relative palaeo-bathymetry and palaeo-discharge-directions. Correlations between the sections have been accomplished by using interpreted seismic data (Line 8307; Schlunegger et al., 1997) and through compilation of ages constrained by magneto-polarity stratigraphies (Strunck and Matter, 2002; Schlunegger, 1996, 1997) and mammal biostratigraphies (Keller, 1989; Engesser, 1990; Jost and Kempf, 2016). Non-dated sections have been correlated with a sequence stratigraphic approach.

We proceeded through detailed sedimentological investigations of key-sites (Fig. 2), which expose the OMM-I succession in proximal (*Entlen-section* east of the *Napf-units*; *Sense-section* west of the *Napf-units*), central (*St. Magdalena-site, Gurten drill core*) and in distal positions (*Mägenwil-site*). The key-sites have been analysed in the field and on digital photos at the scale of 1:50. We categorized the sediments into lithofacies types (e.g. Schaad et al., 1992; Keller, 1989) based on the ensemble of sedimentary characteristics including: grain size, thickness, lateral extent, if applicable, sedimentary structures, basal contact, colour and fossil content. Additionally, the sediments have been analysed according their palaeo-bathymetrical conditions. Please refer to the Appendix for the details of the methodological approaches, the summary of the lithofacies descriptions and interpretation, and for the references to the related articles.

Finally, depositional systems were defined as an ensemble of distinct lithofacies types including the related palaeo-bathymetric conditions. These depositional systems have been mapped at the scale of 1:10'000 at various sites where suitable outcrops were present (see Fig. 2 for visited sites). Published information from deep-drillings (*Boswil 1*; *Hünenberg 1*) and seismo-stratigraphic data (Line 8307; Schlunegger et al., 1997, Line BEAGBE.N780025; Fig. B, Appendix) completed the available database. Palaeo-current directions were measured from the occurrence of imbricated clasts, sole-marks, parting-lineations, orientation of cross-beds and ripple-marks.

3.2 Reconstruction of the chronological framework

The chronological framework of the OMM-deposits in the region has been established by multiple authors through palaeontological analyses of mammal fragments and teeth (Keller, 1989; Schlunegger, 1996; Kempf et al., 1999) and $^{87}Sr/^{86}Sr$ chemo-stratigraphies (Keller, 1989), yielding a numerical age between c. 18.5 and 17 Ma, particularly for the OMM-II (*St. Gallen-Fm*). Subsequent magneto-polarity chronologies (Schlunegger et al., 1996; Strunck and Matter, 2002) paired with further micro-mammal discoveries (Kälin and Kempf, 2009; Jost et al., 2016) allowed to update the chronological framework (Fig. 3) of Keller (1989) through correlations with the Magneto-Polarity-Time-Scale (MPTS) of Cande and Kent (1992, 1995) and the most recent astronomically tuned Neogene time-scale (ATNTS, Lourens et al., 2004). The original correlations of the magneto-zones with the MPTS, or alternatively the ATNTS, were based on the inference that

sedimentation occurred continuously (Schlunegger et al., 1996; Strunck and Matter, 2002). However, based on a reassessment of the magneto-polarity stratigraphy of the *Napf-section* (*Napf-units*, Fig. 3) and further sections in the eastern Swiss Molasse basin, Kälin and Kempf (2009) suggested that sedimentation was possibly interrupted by several hiatuses. Finally, through stratigraphic investigations of the seismic line 8307 (Fig. 2), Schlunegger et al. (1997) proposed that an erosional unconformity and thus a hiatus separates the OMM-I from the OMM-II. Unconformities separating lower- and upper-OMM sequences have not been considered by those authors who established the original chronological framework for the OMM sequences in the region (Keller, 1989; Schlunegger et al., 1996; Strunck and Matter, 2002). Consequently, we reassessed the temporal framework through a compilation of the original and most recent information in the literature, and through mapping and sedimentological investigations.

4 Results and Interpretation

4.1 Revised chronology of the Swiss Molasse sequences

4.1.1 Eastern Swiss Molasse basin

At the eastern proximal basin border, marine sedimentation started with the OMM-I (*Lucerne-Fm*, Fig. 3), which is best presented by the c. 800 m-thick *Entlen-section* (Keller, 1989). There, the overlying OMM-II (*St. Gallen-Fm*) is only 50 m thick, and sedimentation was superseded by the accumulation of fluvial conglomerates of the *Napf*-megafan (*Napf-units*), which gradually replaces the marine strata of the OMM-I c. 20 km farther to the west (Haldemann et al., 1980) upon approaching the *Napf*-megafan apex (Schlunegger and Kissling, 2015; Figs. 3 and 4). This heterochroneity of facies relationships complicates any temporal reconstructions of the OMM sedimentation in the east. Nevertheless, the basal part of the OMM-I follows upon a sharp contact to the underlying USM deposits, as recorded by the *Fischenbach*-section along a river-cut (47°00'14'' N / 8°08'26'' E; Schlunegger et al., 2016). There, the topmost normal magnetozone of the USM is considered to correlate with C6An1 of the MPTS or the ATNTS, respectively (Schlunegger et al., 1996). For the OMM-I, a time interval from MN3a through MN3b (European Neogene mammal units; Mein, 1975; 1979; 1989) has been assigned by Keller (1989) based on micro-mammal records within a section c. 20 km farther to the east (Fig. 3). However, more precise age assignments for the base and the top of this unit are complicated because of a lack of magneto-polarity chronologies. Here, we constrain the age of the basal transgression using two pieces of evidence: First, the transgression post-dates the deposition of the USM, which terminated at C6An1 at the *Fischenbach* (Fig. 3). Second, based on stratigraphic interpretations of palaeo-discharge direction data, Strunck and Matter (2002) considered that the transgression of the OMM progressed from the east towards the west, where the first marine sediments have been dated with C6r in the *Sense-section* (Fig. 3 and 4a; see next section). Accordingly, the onset of the OMM at the *Entlen* predates the transgression at the *Sense*. Based on these arguments, we propose an age of c. 20 Ma for the base of the OMM-I in the eastern Swiss Molasse basin (Figs. 3 and 4).

An age for the top of the OMM-I (*Lucerne-Fm)* can be estimated by using the magneto-stratigraphy of the *Napf-section* (*Napf-units*, Fig. 3) c. 10 km to the west of the *Entlen* (Schlunegger et al., 1996). This section includes an alternation of 6 reversed- and 5 normal-polarized magnetozones. The lowermost, very long normally polarized interval (N1, Fig. 3 and 4a) includes the mammal fossil site *Hasenbach 1* recording an MN3b age (Schlunegger et al., 1996) or even a lower-MN3b age, as a revision of the fossiliferous material has shown (Kälin and Kempf, 2009). This allows a correlation of the normally polarized interval N1 with chron 5En of the MPTS (Cande and Kent, 1992, 1995) or the ATNTS (Lourens et al., 2004), respectively (Fig. 3). Since the third reversed magnetozone of the *Napf-units* is very short (R2), and since the ATNTS chron 5D includes several 100 kyr and is thus quite long, it is most likely that a hiatus encloses C5Dr2 to C5Dr1 (Fig. 3). In addition, because (i) the change from MN3b to MN4a has been calibrated with C5Dr2 (Jost et al., 2016), and since (ii) the base of the overlying OMM-II (*St. Gallen-Fm*; Fig. 3 and 4a) has been dated with MN4 (Keller, 1989), we suggest that the inferred hiatus falls to the boundary between the OMM-I and the OMM-II (Fig. 4). This age assignment is consistent with magneto-polarity stratigraphies in the eastern Swiss Molasse basin (Kempf and Matter, 1999). It is also consistent with micro-mammal investigations in the distal Molasse basin where Jost et al., (2016) found that deposits spanning MN3b and MN4a are missing. Based on these constraints, we suggest that the top of the OMM-I correlates with C5Dr of the MPTS or C5Dr2 of the ATNTS, respectively, followed by a c. 0.5 Ma-long hiatus (Fig. 3 and 4). The overlying magnetozones of the *Napf-units* are correlated with the ATNTS following Sant et al. (2017).

This correlation implies that sedimentation within the OMM-I was continuous, which we justify through the deepening- and shallowing-upward sequence recorded in the *Entlen-section* (see 4.2.1). A maximum flooding-surface (MFS, Fig. 4a), which we infer from the sedimentological analyses across the basin (see 4.2), allows to subdivide the OMM-I into a lower and an upper unit referred to as OMM-Ia and OMM-Ib, respectively (Figs. 3 and 4). It is, that it is possible that sedimentation was interrupted between the OMM-II and the OSM by short intervals (Kälin and Kempf, 2009). The consequences of our refined correlation are a constant sediment-accumulation rate of c. 400 m/Ma from the base to the top of the OMM-I, and the occurrence of a c. 0.5 Ma-long hiatus between c. 18 and 17.5 Ma separating the OMM-I from the OMM-II (Figs. 3 and 4).

In the distal eastern part of the basin, the stratigraphic architecture of the OMM is made of sandstones of the *Lucerne-Fm* at the base, which is overlain by the "Muschelsandstein" unit (Fig. 4b; see 4.2.4) at the top (Jost et al., 2016). Mapping shows that the "Muschelsandstein" near *Mägenwil* (Fig. 2) is c. 5 – 10 m thick and thins towards the depocenter of the *Napf*-megafan deposits to less than 1 m. Correlations of these deposits across the basin have been accomplished through a seismostratigraphic analysis of the seismic line 8307 (Schlunegger et al., 1997; Fig.2). There, the sediments of the OMM-I (*Lucerne-Fm)* onlap onto USM strata and then overlap this unit (Fig. 4b). The overlapping sequence has been referred to as Unit B in Schlunegger et al. (1997), which in turn corresponds to the top of OMM-Ia in our stratigraphic scheme. In addition, our field investigations and micro-mammal correlations (Jost et al., 2016) reveal that the "Muschelsandstein" follows on top of the OMM-Ia and most likely corresponds to the OMM-Ib. Based on these constraints, we suggest that the deposition in the distal basin occurred between c. 19 and 18 Ma (Fig. 4b). However, as visible in line 8307 (Schlunegger et

al., 1997), sedimentation was interrupted at c. 18 Ma by a c. 0.5 Ma-long or possibly longer hiatus. This time span has been specified through new micro-mammal discoveries by Jost et al., (2016) who noted that recorders of MN4a is missing and that the base of the OMM-II (*St. Gallen-Fm)* hosts mammal fragments that correspond to MN4b. The interpretation of an inferred unconformity is additionally supported through observations of vadose cements (Allen et al., 1985) within the "Muschelsandstein", and through evidence for a thick paleosoil separating OMM-I from OMM-II (Fig. 4), as documented mapping near the *Entlen-section* has shown. This information suggests that the uppermost beds of the OMM-Ib (including the "Muschelsandstein") were exposed to erosion after deposition (Allen et al., 1985; Jost et al., 2016). Because of post-depositional erosion of the entire Molasse sequences since the Pliocene (Cederbom et al., 2004; 2011), the continuation of the sedimentary history cannot be constrained.

4.1.2 Western Swiss Molasse

At the proximal basin border in the west, Strunck and Matter (2002) placed the USM/OMM-boundary of the c. 650 m-thick *Sense-section* within C6r of the MPTS (Cande and Kent, 1992; 1995), or alternatively of the ATNTS (Fig. 3; Lourens et al., 2004). The subsequent alternation of normal and reverse magnetozones were correlated by these authors with chrons 6r through 5Dn of Cande and Kent's MPTS (1992; 1995), the latter of which corresponds to C5Dn1 of the ATNTS (Lourens et al., 2004). Following Strunck and Matter (2002), a possible hiatus prior to c. 17.5 Ma (Figs. 3 and 4) is likely to be registered also within the *Sense-section* (Fig. 5b). This implies that a hiatus separates the OMM-I from the OMM-II across the entire basin (Figs. 3 and 4) and that the subsequent sedimentation (base of OMM-II) progressed from the west to the east. The consequences of this chronological framework are a constant sediment-accumulation rate of c. 285 m/Ma during deposition of the western OMM-I, however, sedimentation was possibly interrupted by a short hiatus at the top of the OMM-Ib (Fig. 3).

No micro-mammal sites have been reported so far for the OMM deposits in the western Molasse basin. Therefore, we cannot provide further constraints on the history of sedimentation. However, mapping in the area of *Lake Neuchâtel* (Fig. 2) shows a sedimentary succession similar to the east, where amalgamated sandstone beds are overlain by the "Muschelsandstein" unit. Mapping also shows that these limestones thin from c. 10 m in the *Lake Neuchâtel* area to a few meters towards the distal margin of the *Napf*-megafan (Allen et al., 1985). Because of the architectural similarity to the east, we tentatively consider that the deposition of the "Muschelsandstein" occurred synchronously across the entire Swiss Molasse basin. Similar to the east, however, post-depositional erosion during the Pliocene (Cederbom et al., 2004; 2011) prevents us from presenting any further details on the continuation of the sedimentary history.

4.2 Lithofacies, sedimentary processes and identification of depositional environments

4.2.1 Eastern proximal basin border: Beach sequences with a tidal influence recorded at the Entlen-section

Characterization

We group the 800 m-thick suite of the OMM-I deposits at the *Entlen* (*Lucerne-Fm*) into the two subunits OMM-Ia and OMM-Ib based on differences in the lithological architecture (Fig. 5). The lowermost c. 370 m-thick OMM-Ia is made up of an amalgamation of c. 5 – 10 m-thick tabular sandstone packages with mm- to cm-thick mudstone interbeds. The overlying c. 430 m-thick OMM-Ib sequence comprises an alternation of 2 – 3 m-thick lenticular sandstone beds and dm-thick mudstones layers (Fig. 5a).

The sedimentary suite of the OMM-Ia records a total of 14 lithofacies types (Table 1, Appendix). Fine- to medium-grained sandstones occur as packages of cm- to dm-thick normally graded sequences. These deposits either occur as several m-thick tabular, parallel-laminated units (Sp) that laterally grade into <1 cm-thick cross-beds (Sc), or as several dm-thick low angular cross-bedded units with tangential lower boundaries (Sc). Parallel-laminated sandstone beds also display transcurrent laminations (Sp). These lithofacies associations dominate the OMM-Ia sequence with a relative contribution of >50% (Fig. 5a). Some sandstone beds contain gravels and pebbles in a few places (Sg), and shell fragments (Shf) are visible where sandstone units have erosive bases. A few packages of cross-bedded sandstones (Sct_a) contain current ripple-marks (Scr) at their base, or they have a massive structure (Sm). Centimetre-thick oscillation-ripple marks (Sos-faceis), sometimes with branching crests (Sbr), are present only in some places. The basal contacts of this class of sandstone beds are both erosive and planar (Fig. 5a). Some fine-grained sand- and siltstone interbeds display water escape-structures such as flame-fabrics or sand-volcanoes (Sv). Most of the siltstone beds occur as climbing-ripples (Mcl). The mudstone interbeds are present as mm- to cm-thick parallel-laminated to massive layers (Mp, Mm). Thin mud drapes (Md), a few mm thick, mostly occur on top of current ripple-marks (Scr). In places, root-casts are associated with yellow- to ocherish-mottled colours.

Estimates of palaeo-bathymetric conditions (see Appendix) reveal that the OMM-Ia sediments were deposited in water depths <5 m (Fig. 5a). This is consistent with the inferred near-shore environment (see below; Short, 2012). Measurements of bedform-orientations reveal discharge directions between 315° NW and 60° NE, with a dominant NE-directed transport (Fig. 5a).

The overlying OMM-Ib comprises a total of 9 lithofacies types (Table 1, Appendix). Fine- to medium-grained sandstone packages occur as m-thick lenticular bodies that display several dm-thick low angular trough (Sct_r) or tabular cross-beds (Sct_a). Sct_r-sandstones contain current-ripple marks (Scr) at their base, while laminae-sets of Sct_a-sandstones are interbedded with current-ripples (Scr), which record an opposite flow direction. At one site, dm-thick sandstone with a planar base and a wavy top and with wavelengths of several meters could be assigned to a ridge-and-swale (Srs) structure (Fig. 5a). These lithofacies assemblages contribute to >50% of the sedimentary sequence of the OMM-Ib. Parallel-laminated sandstone beds with transcurrent laminations (Sp) are dm-thick and mainly found at the top of the OMM-Ib unit. In a few places, the sandstones also occur as massive beds (Sm). Mudstone interbeds are dm thick and mostly occur as mud drapes (Md) on top of current ripple-marks (Scr). Ripple- (or lenticular-) and flaser-interbeds (Mle, Mfl) are dm thick and characterized by current ripple-marks with truncated crests. In the *Entlen-section*, the OMM-Ib ends with m-thick palaeo-soils, displaying yellow to reddish mottling, root casts and caliche nodules (Fig. 5a).

Palaeo-bathymetric conditions of the OMM-Ib reveal an increase of water depths to >15 m compared to the OMM-Ia unit (Appendix). This dataset is corroborated with our inferred near-shore- to transitional-environment (see below). The OMM-Ib shallows towards the top and is capped by a thick palaeo-soil. Discharge directions measured from bed-form orientations reveal the full range between 260° W and 70° E (Fig. 5a), which is consistent with the observed bimodal sediment transport of the associated lithofacies types (see below: Sct_a, Sct_r and Scr). Interestingly, dominant discharge directions of the OMM-Ib sediments change towards the N and finally to the W.

Interpretation

The OMM-Ia sediments of the *Entlen-section* are assigned to a near-shore environment, which comprises the lower and upper shoreface where wave activities shape the coastal morphology of a beach (Fig. 5a). Related processes are inferred from the occurrence of tabular, parallel-laminated (Sp) sandstones, which are interpreted to represent sediments of the surf-and-swash zone near the wet beach. Alternatively, this lithofacies association can be placed in the wave-transformation zone where the waves brake. This is particularly the case where these beds laterally grade into <1 cm-thick cross-bedded ripples (Scr) and where normal grading is clearly visible. Low angular cross-beds (Sc) are interpreted to represent sand-reefs, where pebbly-lags (Sg) and shell fragments (Shf) record the occurrence of storm-events. Oscillating-ripple marks (Sos) are presumably formed in the lower shoreface and are evidence for wave-activities (Fig. 5a). Furthermore, these Gp- and Cs-facies are often visible at the base of rip current channels. Water escape-structures, sand-volcanoes (Sv) and climbing-ripples (Mcl), are distinct recorders of fast sedimentation from sediment-saturated water within a wave-dominated beach. In places, the presence of backshore channels (Sc) and floodplains with splays (Sc- and Sm-facies) are inferred where root-casts and incipient pedogenesis are observed (Mp, Mm). Accordingly, these deposits are interpreted to have been deposited in backshore ponds. Contrariwise, tidal processes are related to cross-bedded sandstones (Sct_a) with mud-drapes (Md) on top of the current ripples-marks (Scr). These Md- and Scr-facies, if associated to the Sct_a-sandstones, are distinct features of a slack water stage due to a possible tidal-influence. Alternatively, they might register the occurrence of standing water in a wave-protected area. Root-cast are visible in parallel-laminated (Sp) and massive-bedded (Sm) sandstones and mudstones (Mp, Mm).

The OMM-Ib sediments of the *Entlen-section* are assigned to a near-shore to transitional environment, shaped by the combined effect of wave- and tidal-activities (Fig. 5a). We infer the occurrence of tidal processes by the observation that current ripple-marks (Scr), which are situated on top of lamina sets of tabular- (Sct_a) and trough-cross-beds (Sct_r), point towards an opposite flow direction than the cross-beds themselves (Fig. 5a). In addition, the size of these facies assemblages forming m-scale lenticular shaped sandbodies requires an accommodation space, which is consistent with a lower near-shore setting. In such an environment mud-drapes (Md) on top of the ripple marks are recorders of slack water phases. Finally, lens- (or lenticular-) and flaser-interbeds (Mle, Mfl), both dm thick, are assigned to a similar setting. In contrast, sediment transport by waves is recorded by parallel-laminated sandstones (Sp) with transcurrent laminations, which mark the presence of a surf-and-swash zone. In this context, sandstone beds referred to as ridge-and-swale (Srs) structures could record the

occurrence of high-energetic waves. Furthermore, massive sandstones (Sm) and palaeo-soils with mottled colours, root casts and caliche nodules, mark the presence of a back-shore, possibly terrestrial environment.

In summary, the change of the sedimentary environment within the OMM-I at the *Entlen*, from a near-shore, wave-dominated setting to an environment with tidal records, was associated with a shift towards deeper bathymetric conditions (Fig. 5a). In this context, the deepest inferred bathymetry at the base of the OMM-Ib is assigned to the maximum-flooding surface (MFS) within the OMM-I sequence, which separates the transgressive OMM-Ia from the regressive OMM-Ib (Fig. 6a). This deepening-and-shallowing upward trend is associated with a ~90°-westward rotation of the discharge directions, from an originally unidirectional NE- to an axial NE-SW-directed (MFS) and finally to a transverse N-oriented transport.

4.2.2 Western proximal basin border: Estuarian sequences recording tidal processes at the Sense-section

Characterization

We group the c. 650 m-thick *Sense-section* (Figs. 5b and 3), which comprise OMM-I and OMM-II deposits, into three packages based on distinct facies associations. OMM-Ia deposits are c. 200 m thick and comprise the *lower Sense-beds*. The superseding OMM-Ib sediments are encountered in the *upper Sense-beds* (c. 125 m thick) and the *Kalchstätten-Fm* (c. 275 m thick). The *Sense-section* ends with the *Guggershorn-Fm*, which is c. 50 m thick. Based on our refined chronology (see 5.1 and Fig. 3), we assign this c. 50 m-thick uppermost sequence to the OMM-II.

Within the *Sense-section*, the OMM-Ia is represent as 13 lithofacies types (Table 1, Appendix). Middle to coarse-grained sandstone beds are up to 2 – 3 m thick and massive bedded (Sm). Individual sandstone beds are parallel-laminated (Sp). They also occur as m-scale tabular cross-beds (Sct_a) with well visible top- and bottom-sets and as sequences of cross-bedded troughs (Sct_r). Meter-scale tabular cross-beds (Sc) with sigmoidal geometries contain pebbly lags (Sg) at the bottom-sets and are well exposed along a nearby road-cut (46°49’27” N / 7°18’42” E). Some of these cross-beds contain current-ripple marks (Scr) at the base of Sct_r-sandstones, often draped with a muddy layer (Md). Ripple marks also build up tabular sandstone bodies. In this case the ripples are either asymmetric or symmetric (Sos), and in some cases the crests are branching (Sbr). Mudstone interbeds are 10 – 20 cm thick, massive- (Mm) to parallel-laminated (Mp) and strongly bioturbated (Mf).

Estimates of bathymetric conditions reveal water depths of up to 10 m (Fig. 5b and Appendix). This is consistent with the inferred tidal-dominated environment within an intertidal bathymetry (see below). Measurements of discharge directions reveal a dominant NE-directed sediment transport, which covers the range between c. 0° N and 90° E (Fig. 5b).

The basal part of the OMM-Ib sequence (*upper Sense-beds*, Fig. 3 and Fig. 5b) displays a similar large-scale architecture as the OMM-Ia unit. However, it comprises 4 additional lithofacies types and displays subtle differences: (i) up to 5 – 10 m-thick sandstone beds are normally graded, follow upon an erosive base and display epsilon cross-beds (Sce); (ii) m-scale cross-bedded sandstones (Sct_a) are several meters high and tens of meters wide. Current ripple-marks (Scr), which occur on

top of individual laminae, are draped with mud (Md) and have orientations that imply an opposite flow direction; (iii) medium-grained sandstones show ridge-and-swale structures (Srs) with a small amplitude of a few dm and a large wavelength of several m; they are additionally covered with pebbles (Sg); and (iv) Srs-structures are sometimes also covered with oscillation-ripple marks. This 125 m-thick sequence ends with a c. 20 m-thick succession of mudstones and a c. 15 m-thick amalgamation of sandstone beds. Mudstones are massive bedded (Mm), contain extensive bias (Mf) and are arranged as individual dm-thick packages. Sandstones display massive beds (Sm), with current ripple-marks (Scr) and bioturbation (Sf) in places.

Water depth estimations return values of up to 30 m at the base of the OMM-Ib, which shallow to <5 m further upsection (Fig. 5b). This deepening-and-shallowing trend is consistent with the inferred subtidal environment at the base and higher up in the section (see below). Orientation of discharge directions show an axial, SW-NE-directed transport where they reach the deepest bathymetrical conditions. Sediment transport changes towards a transverse N-directed discharge at the end of the sequence.

The c. 300 m-thick upper part of the OMM-Ib (*Kalchstätten-Fm*) (Figs. 3 and 5b; Strunck and Matter, 2002) displays two major differences (Table 1, Appendix): (i) dm-thick mudstone interbeds appear more frequently; and (ii) alternations of sandstone- and mudstone-beds are interfingering with m-thick massive- to cross-bedded conglomerates (Gm, Gc). The sedimentary suite thus starts with 5 – 10 m-thick sandstone beds, which are massive (Sm), tabular cross-bedded (Sct_a) and trough cross-bedded (Sct_r). Sandstones also display tabular geometries and contain bioturbation in places (Sf). Occasionally, current-ripple marks (Scr) are draped with mud (Md). Up to m-thick, massive-bedded conglomerates (Gm), sometimes only visible as dm-thin pebbly-lags interbedded in sandstone beds (Sg), appear approximately in the first quarter of this sequence and are embedded in massive-bedded mudstones (Mm) and sandstones (Sm). The conglomerates then change towards several m-thick, massive- (Gm) and cross-bedded geometries towards the top of the section (c. 50 m-thick OMM-II).

No quantitative data are available to define bathymetric conditions. Nevertheless, sandstones at the base of this unit display similarities to the sedimentary architecture of the subtidal shoals at *St. Magdalena*, where water depths of c. 5 m are estimated (see below). We thus suggest subtidal conditions for the base of this unit. A shallower bathymetry is inferred from the occurrence of conglomerates in the OMM-II suite, possibly deposited within coarse-grained rivers in a backshore environment at the top where conglomerates start to dominate the sedimentary suite. Measurements of palaeo-currents from imbricated clasts (Strunck and Matter, 2002) reveal a transverse to W-directed sediment discharge, which is consistent with own observation, covering the full range between 230° SW and 330° NW.

Interpretation

We assign the OMM-Ia (*lower Sense beds*) to an intertidal environment bordered by deltas, estuaries and tidal-flats (Fig. 5b). This is inferred from the occurrence of sigmoidal cross-bedded sandstones (Sc) with distinct top-, fore- and bottom-sets, which also contain pebbly-lags (Sg) at their base. These facies assemblages are characteristic for deposits of a Gilbert-Delta

(e.g. Bates, 1953). In this context trough cross-bedded sandstones (Sct_r) and possibly massive bedded (Sm) units can be assigned to mouth-bar deposits where estuaries end, or alternatively to tidal inlets. The presence of current-ripple marks (Scr) with mud-drapes (Md) at the base of tabular cross-beds (Sct_a) can be assigned to an intertidal setting, where ripple-marks record the activity of tidal-currents, while mud-drapes form during slack phases. Additionally, ripple-marks (Sos) with branching crests (Sbr) and parallel-laminated sandstones (Sp) were most likely formed in shallow water conditions, possibly under the influence of waves. The massive-bedded (Mm), parallel-laminated (Mp) and strongly bioturbated (Mf) mudstone interbeds are assigned to a tidal flat.

The sandstones with cross-beds (Sc) encountered at the base of the OMM-Ib (*upper Sense-beds*) are assigned to tidal channels, where epsilon cross-beds (Sce) are records of slip faces of meanders. In support of the inferred recorders of tides, meters-high cross-bedded sandstones (Sct_a) with draped (Md) current-ripple marks (Scr) on top of sandstone laminae are distinct characteristics for tidal sandwaves. In this context, the several tens of m-wide sandwaves are possibly formed in a subtidal environment. In contrast, the occurrence of wave activities is inferred from m-scale ridge-and-swale (Srs) structures and oscillating-ripple marks (Sos). Likewise, pebbly layers (Sg) among the Srs-sandstones are evidence for high-energetic storms. These two latter lithofacies (Sct_a, Srs) record the deepest bathymetrical point of the Sense section. Massive bedded (Mm) mudstones and sandstones (Sm) with bioturbation (Mf, Sf), which are encountered at the end of the lower part of the OMM-Ib, are assigned to a tidal mud- and sand-flat environment.

The upper part of the OMM-Ib (*Kalchstätten-Fm*) is assigned to a regressive, shallow marine sequence. Similar to the OMM-Ia unit, we assign the OMM-Ib deposits to an environment with estuaries bordered by subtidal shoals and possibly tidal-flats. The occurrence of estuaries is inferred from cross-bedded sandstones (Sct_a) superimposed with current-ripple marks (Scr) and mud-drapes (Md). In such an environment, cross-bedded troughs (Sct_r) with massive-bedded sandstones (Sm) could represent mouth-bar deposits at the end of estuaries or tidal inlets, which laterally grade into subtidal shoals (Sct_r). Bioturbated sandstones (Sf) could either be assigned to a tidal sand-flat environment or are records of organisms within subtidal conditions. Massive- and cross-bedded, a few m-thick conglomerates (Gm, Gc), which are embedded within massive-bedded mudstones and sandstones (Mm, Sm), are assigned to distal recorders of floods, where gravels were supplied by a stream with sources in the Alps. In this context, conglomerates are also only visible as a dm-thin layer among sandstones (Sg). Up-section, the conglomerate beds become more frequent and more continuous and display several m-thick beds, with massive- to cross-bedded geometries (Gm, Gc). These deposits are assigned to coarse-grained rivers interfingering with the Burdigalian sea (Strunck and Matter, 2002) and finally correspond to the OMM-II and its terrestrial equivalent (*Guggershorn-Fm*).

In summary, the *Sense-section* (OMM-I and OMM-II) records a distinct change of the sedimentary environment and bathymetrical conditions. The deposits of the OMM-Ia show a transition from an estuarian- towards a subtidal-environment. Largest water depths are inferred from deposits at the base of the OMM-Ib, which is thus likely to represent the maximum-flooding stage (MFS) of the OMM-I. The sediments encountered towards the top of the OMM-Ib are assigned to water

depths within a subtidal-to intertidal bathymetry. Measurements of discharge directions in this large-scale deepening-and-shallowing upward cycle reveal a shift from a transverse NE-directed sediment transport to an axial SW-NE-directed transport (MFS) and finally to a N-directed discharge at the top of the OMM-I.

The overlying conglomerates, deposited within fluvial streams forming a deltaic environment (OMM-II and then OSM), record a shallowing-upward sequence, evolving towards a braidplain towards the top. There, measurements of palaeo-currents reveal a W-directed discharge direction (Strunck and Matter, 2002), which is associated with a ~90°-westward rotation in comparison to the OMM-Ib.

4.2.3 Central proximal basin border (Napf-units): Alluvial megafan deposits

Characterization

The *Napf-section*, which is a terrestrial equivalent of the OMM g[illegible]p (Figs. 3 and 4; Schlunegger et al., 1997), is c. 1550 m thick and includes a succession of conglomerates, sandstones and mudstone interbeds (Matter, 1964), which are categorized into 5 lithofacies types (Table 1, Appendix). Individual conglomerate se[illegible]ces are up to 10 m thick and display stacks of 2 – 3 m-thick beds with massive (Gm) to cross-bedded (Gc) geometries. The sandstone beds occur as massive bedded (Sm) and cross-bedded (Sc) units. T[illegible] interbedded mudstones display a tabular (M[illegible]) fabric and have a yellowish-reddish mottling, caliche nodules and root c[illegible]. Palaeo-flow measurements based on orientations of so[illegible]rks imply a NE-directed transport during USM-times (Schlunegger et al., 1997). C[illegible] measurements of imbricated clasts reveal a change from a NE- to a NW-direction between OMM-I- and O[illegible]SM-times.

Interpretation

We interpret the association of massive (Gm) to cross-bedded (Gc) conglomerates and massive- to cross-bedded sandstones (Sm, Sc) as deposits within a braided river system (Table 1, Appendix). In such an environment, conglomerates are common recorders of active channels. Massive- (Sm) to cross-bedded (Sc) sandstones alternating with mottled mudstones were most likely formed during bursts of channel belts, thereby forming creva[illegible]splay deposits (Platt and Keller, 1992). Mudstone interbeds (Mp) with evidence for palaeo-soil genesis formed when channel belts shifted away from the axis of the section (Platt and Keller, 1992). This facies-association was mapped over tens of kilometres, both across and along strike of the basin orientation. It is thus assigned to an alluvial megafan (Schlunegger and Kissling, 2015).

4.2.4 C[illegible]ntral basin (St. Magdalena, Gurten): Subtidal shoal deposits

Characterization

Outcrops within a cave-system near *Fribourg* (*St. Magdalena*; Fig. 2) reveal 3D-insights into several m-thick sandstones with cm-thick mudstone interbeds. The sandstones are medium- to coarse -grained and display an amalgamation of 1 – 3 m-

wide, cross-bedded troughs (Sct_r) with current-ripple marks (Scr) at their base that are covered by mud-drapes (Md). The amplitude of the troughs is in the range of several dm, while the cross-sectional widths span several decimetres to meters. The sandstones also occur as massive-bedded units (Sm). They are occasionally interbedded with current-ripple marks (Scr) draped with mud layers (Md). Basal contacts are mostly erosive. In the nearby c. 260 m-thick *Gurten* (Fig. 2) drill core (Fig. C, Appendix), related deposits occur as cross-bedded sandstones (Sc) topped with mud-drapes (Md). These lithofacies associations (Table 1, Appendix) are most abundant within the drill core and make up c. 200 m of the log. However, because drill cores offer limited information about the dimensions of the encountered sediments, we were not able to determine if cross-beds can be assigned to tabular-beds (Sct_a) or to troughs (Sct_r).

Measurements of morphometric properties (*St. Magdalena*; Fig. 2*)* allow an estimation of water depth in the range between c. 3 and 5 m (Table 2, Appendix), which is consistent with a inferred subtidal-shoal environment (see below). Discharge directions measured at *St. Magdalena* reveal a WSW-ESE-dominated sediment transport. However, we were not able to carry out quantitative measurements for the *Gurten* (Fig. 2) drill core, neither for bathymetrical conditions, nor for discharge directions for the reasons mentioned above.

Interpretation

The several m-thick outcrops near Fribourg are interpreted as sediments of subtidal shoals. The m-scale cross-bedded troughs (Sct_r) with current-ripple marks (Scr) at their base record the occurrence of currents within a subtidal environment and are interpreted as sand-dunes or megaripples. Alternatively, sandstone troughs (Sct_r) could be assigned to a mouth-bar environment, where massive-bedded sandstones (Sm) would represent recorders of fast sedimentation. Truncated crests of current ripple-marks (Scr) record the erosion through strong currents. In contrast, mud-drapes (Md) on top of the ripple-marks formed during low-energy tides, or possibly during slack stages. Similar deposits (Sct_r, or possibly Sct_a) within the *Gurten* drill core could also be interpreted as sediments of subtidal shoals, however, due to limited exposure, interpretations are non-conclusive.

Water depth estimations (see Appendix) reveal shallow bathymetrical conditions (3 – 5 m) within a subtidal-shoal environment. Discharge directions are assigned to an axial, WSW-ESE-directed transport, which is consistent with a tidal-dominated environment where bidirectional sediment transport occurs.

4.2.4 Western and eastern distal basin border (Lake Neuchâtel and Wohlen area): Coarse-grained shelly sandstones and coarse-grained sandstone sequences

Characterization

Large-scale coarse-grained sandstones where individual grains might be larger than 2 mm are found along strike in the distal part of the basin between the *Lake Neuchâtel* and around the *Wohlen area* (Fig. 2). These deposits are either calcareous-sandstones with shelly-fragments (Scc) also called the “Muschelsandstein” of the OMM-Ib (Allen et al., 1985: Fig. 4b).

Alternatively, they are referred to the coarse-grained sandstones with large litho-clasts (Slc), also called the "Grobsandstein" (Jost et al., 2016), where coquinas and shell-fragments are missing.

Calcareous, shelly-sandstones (Scc) occur at distal sites in the western and eastern Molasse basin and are an assemblage of various lithofacies (Table 1, Appendix). This Scc-facies association is made up of 5 – 10 m-thick, coarse-grained sandstone beds with low-angle cross-beds (Sc). They contain coquinas and shell-fragments (Shf) and pebbles (Sg) in places. Interbedded fine-grained sandstones contain current-ripple marks (Scr) recording opposite flow direction in relation to the cross-beds (Sc). Mapping shows that in the west (near *Lake Neuchâtel*, Fig. 2), the Scc-"Muschelsandstein" deposits are c. 5 m thick and record NNE- to NE-directed sediment transport. Foreset heights of these deposits thin to <1 m towards the front of the *Napf*-megafan, where herringbone cross-beds imply SW-NE-directed, bi-modal sediment transport. Farther to the NE, Scc-"Muschelsandstein" deposits grade into Slc-"Grobsandstein" units (Jost et al., 2016), which show m-high tabular cross-beds (Sct_a) or dm-high trough cross-beds (Sct_r) with m-wide diameters. Measurements of palaeoflow directions reveal a SW- and SE-directed transport. These deposits are either time-equivalents of the Scc-"Muschelsandstein" and thus constitute the OMM-Ib sequence, known observation imply. Alternatively, they also mark the base of the OMM-II sequence (Jost et al., 2016).

"Muschelsandstein" deposits are also found in the eastern distal basin near the *Wohlen* area, where foresets of cross-beds are 6 to 8 m and in some locations up to 10 m high (Allen et al., 1985). In contrast to the deposits near the *Lake Neuchâtel*, discharge directions are oriented towards the SSW covering the range between 230° and 250° and striking parallel to the topographic axis. Estimations of water-depths of the Scc-"Muschelsandstein" reveal palaeo-bathymetric conditions (Table 2, Appendix) between 60 and 100 m, consistent with calculations by Allen et al. (1985).

Interpretation

The Scc-"Muschelsandstein" sediments are related to tidal deposits along the northern margin of the Burdigalian seaway (Allen et al., 1985, Jost et al., 2016). Cross-beds (Sct_a) reveal deposition under strong tidal currents (Allen et al., 1985). These deposits are thus assigned to offshore sand-waves dominated by strong tides, where sediment transport was NNE- (*Lake Neuchâtel*) or SSW-directed (*Wohlen* area, Fig. 2). In places, pebbly-lags (Sg) are interpreted as flood-related supply of gravels into the offshore-environment. Contrarywise, the coarse-grained sandstones (Slc-"Grobsandstein" sediments) reveal similarities to the subtidal-shoal deposits encountered at *Fribourg* where trough cross-bedded sandstones (Sct_r) and tabular cross-beds (Sct_a) dominate the facies assemblages. However, the deposits in the *Wohlen* area are coarser-grained, and cross-beds have larger diameters, but similar thicknesses. We relate the coarse-grained nature of the deposits to the proximity of the *Napf*-megafan in the SW. The cross-beds with larger wavelengths and similar amplitudes possibly imply stronger currents compared to the subtidal shoal-deposits near *St. Magdalena*.

5 Evolution of depositional environments

As outlined in the previous sections, the lithofacies-types encountered in the key sections can be assembled, and thus grouped, into 7 depositional environments including terrestrial environments and megafans, beaches and estuaries, nearshore to shoreface environments, offshore conditions and subtidal shoals. These depositional environments were mapped within the central Swiss Molasse (see Fig. 2 for sites) according to the criteria outlined above. This section presents the results in the form of four paleogeographic maps (Figs. 6a to d).

5.1 USM

During USM-times, prior to the Burdigalian transgression, the basin was occupied by alluvial megafans at the proximal basin border, which gave way to an axial-directed meander-belt environment in the distal basin (Fig. 6a). Palaeo-discharge measurements of sole marks (Schlunegger et al., 1996; this work) and analysis of heavy-mineral assemblages (Füchtbauer, 1964) revealed a NE-directed material transport (Fig. 3) towards *Munich* (Fig. 1). There, the Molasse streams ended in a peripheral sea where neritic- to open-marine environmental conditions prevailed (Kuhlemann and Kempf, 2002). A possible drainage divide was situated somewhere SW of *Geneva* (Allen et al., 1991; Strunck and Matter, 2002), which may have separated a southward-oriented discharge to the Tethys in the S, from a northward-directed transport to the Paratethys in the NE (Allen et al., 1985). However, the details on the drainage system at that time are not clear, particularly for the region SW of *Geneva* (Fig. 6a).

5.2 OMM-Ia

The palaeogeographic situation at c. 20 – 19 Ma is shown in Fig. 6b. It illustrates that the central part of the Molasse basin changed to a peripheral sea, which was c. 40 km wide. Palao-bathymetrical conditions revealed water depths that correspond to a subtidal- to nearshore-environment (see Appendix). Nearshore to possibly offshore bathymetrical conditions (30 – 50 m) are recorded by subtidal mega-sandwaves (Allen and Bass, 1993) south of *Lake Geneva* and by the predominant occurrence of sandstone-mudstone-alternations within the *Wohlen* area in the NE (Fig. 2), where OMM-Ia deposits were encountered through drilling (Schlunegger et al., 1997). Farther to the NE, palaeogeographic reconstructions by Kuhlemann and Kempf (2002) imply that the nearshore to possibly offshore conditions at the *Wohlen* area changed to an open, possibly deep-marine environment near *Munich*. Subtidal shoals, up to 5 m deep, occupied the western part of the central Swiss Molasse (Fig. 6b). These deposits separated the deeper nearshore environments on both sides, and thus acted as a divide within this peripheral sea. The inferred divide is also corroborated by data about drainage directions (Allen and Bass, 1993; this work; Fig. 6b). Measurements of sediment transport directions from the shoal deposits themselves (cross-beds) reveal a bi-modal, SW-NE-directed transport, with a dominant NE-orientation at the proximal basin border where deltaic foresets accumulated within an estuarine environment. Mapping allowed to trace the shoal deposits towards the northern tip of the *Napf*-megafan, from where the shoals narrow from c. 20 km to c. 10 km over a 70 km-long distance along strike. It thus appears that the shoals

were deflected to the proximal southern basin border and thus towards the topographic axis through a dominant NE-directed material transport (Fig. 6b). This statement is supported by measurements of transport direction of the *Napf*-megafan (i.e. clast imbrications) and the coastal deposits at the *Entlen* (i.e. parting-lineation, cross-beds) pointing material transport towards the NE (Figs. 3 and 6b). At the distal margin of the basin, beach sandstones gave way to subtidal-shoal deposits up-section. South of *Lake Geneva*, sediment discharge was oriented towards the SW (i.e. foresets from subtidal sandwaves and trough cross-beds; Allen and Bass, 1993; Fig. 6b). It appears, that the central Swiss Molasse was a region of sediment export, which was accomplished through strong tidal currents (Bieg et al., 2008).

5.3 OMM-Ib

The situation during c. 19 – 18 Ma includes the maximum-flooding period (MFS). This time was characterized by a deepening and widening of the basin to depths > 50 m and widths up to 80 km (Fig. 6c). In comparison to the OMM-Ia prior to the maximum-flooding conditions, the alluvial megafans at the proximal basin margin experienced a backstepping. This is inferred from the bi-modal E-W-orientation of material transport measured from the nearshore sand-waves at the *Entlen* section, which imply a free-passage for tidal currents along the basin margin (Fig. 6c). Additionally, a deepening of the basin is inferred from the absence of subtidal shoal deposits, or at least from the shifting of this depositional system to the close proximity of the *Napf*-megafan. Also in contrast to the OMM-Ia, the topographic axis shifted towards the distal basin margin where offshore conditions prevailed (Fig. 6c). There, measurements of sediment discharge in the distal east (*Wohlen* area) reveal a SW-directed transport, while sediment transport in the distal west (*Lake Neuchâtel* area) was directed towards the NE. Both point towards a possible depocenter at the northern tip of the *Napf*-megafan (see also Allen et al., 1985). Farther to the east in the Munich area, the offshore marine environment changed to shallow marine conditions (Kuhlemann and Kempf, 2002).

5.4 OMM-II to OSM

The palaeogeographic situation shown in Fig. 6d comprises the time-span between c. 18 and c. 14 Ma and displays the evolution from the OMM-II to the OSM. The OMM-II period followed up a period of erosion and non-sedimentation across the entire basin (see also Figs. 3 and 4). This is inferred from a hiatus encountered within the *Napf*-units (this work, Kuhlemann and Kempf, 2009), seismic lines in the *Wohlen* area (Schlunegger et al., 1997), vadose cements found in the "Muschelsandstein" (Allen et al., 1985) and the best-fit correlation of the magnetopolarity stratigraphy in the proximal west (Figs. 3 and 4). In addition, measurements of discharge direction reveal SW-oriented sediment transport at proximal positions. This also implies that a possible drainage divide had to shift towards the NE and could have been situated somewhere near *Munich* or possibly farther east. We infer this from the supply of material with sources in the Hercynian basement north of Munich (Fig. 1) or the *Bohemian* massif ("Graupensandrinne"; Allen et al., 1985; Berger et al., 2005), which implies a westward orientation of the basin axis. This is consistent with the orientation of the (palaeo-) "Glimmersandrinne" (Berger, 1996) pointing towards the SW (Fig. 6d). This period ended with the progradation of the

alluvial megafans during the time of the OSM, while measurements of discharge directions reveal a NW-oriented transport (Schlunegger et al., 1997; Kuhlemann and Kempf, 2002; Strunck and Matter, 2002; this work).

5.5 Evolution from USM to OSM

In summary, the establishment of the Burdigalian seaway was accompanied by a change in discharge directions, from an originally NE- (USM- and OMM-Ia-times; Figs. 6a and b) to a N- to NW-directed transport with a strong bidirectional (SW-NE) tidal contribution (OMM-Ib- and OMM-II-times (Fig. 6c), and finally to a NW-oriented discharge (OSM-times; Fig. 6d). Additionally, the Burdigalian transgression is related to a deepening and widening of the basin, including a northward shift of the topographic axis to the distal basin margin, where offshore marine conditions established. This shift towards marine conditions was also associated with a change from an overfilled (USM) to an underfilled (OMM) basin. Furthermore, during OMM-I-times, the central Swiss Molasse acted as a final sedimentary sink situated in front of the *Napf*-megafan. This situation changed during the subsequent OMM-II- and particularly during OSM-times, when the basin became overfilled. At that time, a large fraction of the supplied material became exported towards the SW. These observations point to an incipient tilt of the orientation of the basin axis from the NE to the SW between the OMM-I and the OMM-II. In support of this interpretation, OMM-I sedimentation started slightly earlier in the east than in the west, implying a westward-transgression at 20 Ma (see also seismic line BEAGBE.N780025 in the Appendix, Fig. B), while the opposite occurred after c. 18 Ma during the transgression of the OMM-II when the sea progressed from the west to the east.

6 Discussion

The Burdigalian transgression of the OMM could be explained by a surface control, where a reduction of supplied sediment volumes (Schlunegger, 1999; Kuhlemann et al., 2001, 2002; Willet, 2010) in combination with an eustatic rise of the sea level (Keller, 2012; Reichenbacher et al., 2013; Pippèrr and Reichenbacher, 2017; Miller et al., 1998; Zachos, 2001) have been proposed as plausible mechanisms for an ingression of the peripheral sea to the Swiss part of the Molasse basin (Allen et al., 1985). As will be discussed below, we consider that a reduction of sediment supply rates paired with eustatic variations of the sea level could have contributed to the shift towards an underfilled stage of the basin and the formation of several hiatuses. In addition, we will argue that the uplift of the *Aar-massif* and the related subduction processes of the European slab (Herwegh et al., 2017) have most likely been linked with the changes in the basin geometry at the scale of the Swiss Molasse basin. However, these controls are not capable of explaining reversals of discharge directions from the NE to the SW at the scale of the entire basin at least between *Munich* and *Geneva* and beyond (Kuhlemann and Kempf, 2002), which ask for a tectonic control situated at deeper crustal levels. Pfiffner et al. (2002) explored these mechanisms and proposed that the drainage direction reversal occurred in response to a tilt orientation of European foreland plate caused by shifts in the tectonic loading at the crustal scale, which is presented in the next section.

6.2 Stratigraphic signals related to lithospheric-scale processes: The reversal of the drainage direction

An interpretation of the drainage reversal requires an overview of the history of the NAFB at a larger spatial and temporal scale. This is presented in this section, but we acknowledge that further research is needed to fully support the interpretation of a possible lithospheric control.

Between 33 and 30 Ma beneath the Central Alps of Switzerland, the continental lithosphere of the European plate entered the subduction channel underneath the Adriatic continental plate (Schmid et al., 1996; Kissling and Schlunegger, 2018), while subduction of the European oceanic lithosphere continued beneath the eastern Alps, as palinspastic restorations reveal (Handy et al., 2015). Strong tension forces started to operate at the stretched margin of the European continental crust particularly beneath the Central Alps (Schlunegger and Kissling, 2015) with the result that the subducted oceanic lithosphere of the European plate broke off (Davies and von Blanckenburg, 1995). The consequence was a rebound of the European plate, a rise of the Swiss Alps and an increase in sediment flux to the Swiss Molasse basin (Sinclair, 1997; Kuhlemann et al., 2001; Willett, 2010; Garefalakis and Schlunegger, 2018), which finally became overfilled at c. 30 Ma (Sinclar and Allen, 1992; Sinclair, 1997). East of *Munich*, however the basin was still underfilled as testified by deep marine sedimentation, where debris flows and proximal turbidites accumulated within the basin axis (Fertig et al., 1991; Malzer et al., 1993; Lu et al., 2018). We use these observations to propose that vertically directed slab-load forces were still downwarping the foreland plate beneath the eastern margin of the Eastern Alps. This most likely resulted in a stronger deflection of the European plate beneath the Eastern Alps compared to the Central Alps, which could explain the east-directed sediment transport prior to c. 20 Ma (Fig. 6a). Between c. 20 – 17 Ma, i.e. during OMM-times, a remarkable change was recorded in the Molasse basin. The eastern Molasse basin experienced a change from deep to shallow marine conditions (Kuhlemann and Kempf, 2002), while the Swiss Molasse basin recorded a reversal of the drainage direction from the E to the W, and material with an eastern provenance signal was supplied to the Swiss Molasse basin through the "Graupensandrinne" (Kuhlemann and Kempf, 2002). We relate these observations to changes in the slab-load forces along strike. Particularly, in the eastern Molasse basin, the change from deep to shallow marine conditions could reflect the occurrence of slab unloading (Ustaszewki et al., 2008), while slab downwarping beneath the Central Alps of Switzerland continued (Kissling and Schlunegger, 2018), and was possibly accelerated, as will be outlined in the next section. We suggest that the inferred along-strike differences in the slab geometry resulted in a tilt of the basin axis towards the west, which is shown in the reversal of the drainage direction between 20 and 18 Ma.

6.3 Stratigraphic signals related to crustal-scale processes: The uplift of the Aar massif and the widening of the Swiss Molasse basin

During the Burdigalian, a short phase of fast exhumation (Boston et al., 2017; Schlunegger and Willet, 1999), which occurred in the *Lepontine* area situated in the central Alps of Switzerland (Spicher, 1980), was associated with an uplift pulse of the *Aar-massif* situated farther north (Herwegh et al., 2017; Fig. 2). Kissling and Schlunegger (2018) proposed a mechanism referred to as roll-back subduction as an explanation for these observations. According to these authors,

delamination of crustal material from the European mantle lithosphere along the Moho resulted in a stacking of buoyant lower crustal rocks beneath the *Lepontine dome* and the *Aar-massif* forming the crustal root (Fry et al., 2010; Fig. 1b). These processes are considered to have maintained the isostatic equilibrium between the crust and the subducted lithospheric mantle and thus the elevation of the topography (Schlunegger and Kissling, 2015) and they most likely balanced, through the stacking of the crustal root (Fry et al., 2010, Fig. 1b), the fast removal of upper crust material in the *Lepontine* area at that time (Schlunegger and Willet, 1999; Boston et al., 2017). Delamination of crustal material was also invoked to explain the rapid exhumation and northward thrusting of the *Aar-massif* along steeply dipping thrusts at c. 20 Ma (Herwegh et al., 2017). This process was most likely accompanied by a short period of fast roll-back subduction of the European mantle lithosphere, which was recorded in the Swiss Molasse basin by a 20 – 40 km northward shift of the distal basin border (Schlunegger and Kissling, 2015; Fig. 1b). We use these mechanisms to explain the widening and a deepening of the basin in the central Swiss Molasse, giving way to the deposition of the offshore "Muschelsandstein" (Figs. 6b and 6c) particularly during OMM-Ib times. Interestingly, this lithofacies association has been mapped along the distal basin border adjacent to the external massifs only.

In the *Aar-massif*, structural mapping (Wehrens et al., 2015; 2017) revealed that this crustal block was rising along steeply SE-dipping thrust faults (Fig. 1b). Accordingly, the delamination and the rise of the *Aar-massif* (Herwegh et al., 2017) also resulted in the build-up of topographic loads and the subsequent re-routing of the drainage systems (Kühni and Pfiffner, 2001) within the Central Alps. We suggest that the effects related to the rise of the *Aar-massif* are also registered in the basin sedimentology at a smaller scale through subtle details. Sinclair et al. (1991; 1996; 1997) explored these stratigraphic responses through the application of a linear elastic plate model where thrusting and erosion are dynamically coupled. In their model, the distance between the location of thrusting (*Aar-massif*) and the site in the basin where a signal is expected depends primarily on the mechanical strength of the foreland plate (Sinclair, 1996). The flexural rigidity of the plate underlying the Swiss Molasse basin has been quantified with an elastic thickness ranging between 10 – 30 km based on the curvature of the foreland plate beneath the Swiss Molasse basin (Sinclair et al., 1991; Pfiffner et al., 2002). For a foreland plate with these properties, shifts in surface loads through the km-thick stacking of additional material (*Aar-massif*) is likely to result in the formation of several tens of meters of supplementary accommodation space at the proximal basin border. As a result, depocenters are predicted to backstep to proximal positions, which is consistent with our observations. In addition, according to Sinclair (1996), upward-directed bulging of a few tens of meters is expected at the distal (forebulge) and at the lateral margins of the load (lateral bulge). The spacing between an expected lateral bulge and the location of the surface forcing ranges between 50 – 100 km, which is consistent with the distance between the *Aar-massif* and the inferred subtidal-shoals in the western Swiss Molasse basin (near *Fribourg*; Figs. 2 and 6b). Because the plate had an eastward tilt at that time, as inferred from palaeo-flow directions, such a flexural signal could possibly not be recorded to the east of the *Aar-massif* as the marine conditions were too deep (Figs. 6b and 6c). We also use these mechanisms to explain the establishment of different depositional environments at the proximal basin border of the Swiss Molasse Basin. East of the *Napf*-megafan a relatively late subsidence (rate of c. 400 m/Ma) most likely resulted in a steeper submarine gradient compared to the west,

where the inferred bulging lowered and subdued the submarine slopes (subsidence rate of c. 285 m/Ma). This could explain why the operation of waves is predominantly recorded along the eastern proximal steeper basin margin. Indeed, investigations on modern coasts have shown that steeper coasts tend to promote the formation of larger waves (Flemming, 2011). In contrast, in the western Swiss Molasse, estuaries and tidal-channels could establish as the wave energy decreased in the subdued coastal landscape. Note, we cannot fully exclude that basement uplift, which causes modern irregularities in the contour lines of the Molasse base in western Switzerland (Spicher, 1980), was shifting the peripheral sea to shallower bathymetries also during OMM-times. If such a mechanism did occur, then it could have amplified the effects related to flexural bulging.

In summary, we suggest that the delamination of the *Aar-massif* and the associated roll-back subduction of the European mantle lithosphere had two superimposed effects: It resulted in a widening and deepening of the basin particularly at distal sites, giving way to an offshore seaway where the "Muschelsandstein" accumulated and resulting in the establishment of a depositional sink situated to the north of the *Aar-massif* (Fig. 6c). However, it also resulted in a buckling of the foreland plate through shifts in the surface loading, thereby amplifying the subsidence at the proximal basin border, but subduing the submarine topography through the formation of a lateral bulge where subtidal shoals could establish.

6.4 Stratigraphic signals related to surface controls: Eustatic and sediment flux changes recorded by several hiatus and changes to marine conditions

While tectonic processes are registered in the arrangement of depositional systems in the entire Swiss Molasse basin, signals related to eustatic changes of the sea level are recorded mainly by several hiatus (Figs. 4a and 7). In this context, $\delta^{18}O$-values measured on benthic foraminifera have been used as proxy for establishing patterns of sea level changes (Miller, 1998). In particular, a shift to more positive values of the stable oxygen isotope $\delta^{18}O$ implies a growth of polar ice sheets, where lighter oxygen isotopes ($\delta^{16}O$) are preferentially stored (Zachos, 2001). As a consequence, the global sea level most likely decreased during shifts towards heavier (and thus positive) isotopic records in planktonic organisms (Miller et al., 1998). These patterns have been reconstructed by Miller et al. (1996; 1998) at a high resolution. Interestingly, shifts towards larger $\delta^{18}O$ values generally coincide with times when hiatus are registered in the Molasse basin (Fig. 7; see also Pippèrr and Reichenbacher, 2017; Sant et al., 2017). We thus suggest, that even small drops in global sea level initiated a phase of erosion and recycling of previously deposited sediments because of the proximity of the Swiss Molasse to the peripheral seas. As a more prominent signal, it is possible that a reduction in the supply rates of sediment to the Swiss Molasse basin contributed to the shift towards marine conditions (Fig. 7). Kuhlemann et al. (2002) quantified volumes of sediments preserved in the circum Alpine basin (with subsequent modifications by Willett, 2010) and identified the fluxes of material with sources in the Alps. According to the sediment budgets of these authors, the Burdigalian transgression at c. 20 Ma was associated with a c. 30 – 40 % reduction of the supply rates of sediment from the Central Alps to the Swiss Molasse basin, from 25'000 km^3/Ma prior to c. 20 Ma to c. 15'000 km^3/Ma thereafter (Fig. 7). The mechanisms leading to this reduction in surface mass fluxes are not fully understood (Kuhlemann et al., 2002), and multiple hypotheses have been proposed

including: (i) shifts towards a dryer climate paired with a widespread exhumation of crystalline rocks and a reorganisation of the drainage network in the Central Alps (Schlunegger et al., 2001), (ii) tectonic extension along the Simplon detachment fault which could have lowered the surface topography in the Swiss Alps (Kuhlemann et al., 2001), and (iii) changes in the tectonic forcing where the uplift of the *Aar-massif* resulted in a rerouting of the Alpine streams and a reduction in their erosive power (Kühni and Pfiffner, 2001). Irrespective of the proposed mechanisms, the reduction of the supply rates of sediment most likely contributed to the establishment of marine conditions in Switzerland. In this context, an increase in sediment fluxes after c. 17 Ma (Kuhlemann et al., 2002) could have resulted in the shift from marine to continental sedimentation giving way the OSM.

7 Summary and Conclusion

In summary, we suggest that the Burdigalian transgression was controlled through the combination of a deepening and widening of the basin and a reduction of the supply rates of sediments, which we ultimately relate to tectonic processes in the Alpine hinterland. In this context, roll-back subduction of the European mantle lithosphere, delamination of crustal material and the associated rise of the *Aar-massif* (Herwegh et al., 2017) most likely responsible for the widening of the basin in the foreland (Schlunegger and Kissling, 2015). In the Alpine hinterland, these processes occurred simultaneously with a slip along the *Simplon* detachment fault and thus with a change in the configuration of exposed lithologies (Schlunegger et al., 2001; Kühni and Pfiffner, 2001), with the consequence that the sediment fluxes to the basin decreased. In addition, shifts in surface loads caused by thrusting of the *Aar-massif* resulted in flexural adjustments in the Molasse basin, which could explain the establishment of distinct depositional environments and the formation of subtidal-shoals where a lateral bulge is expected. Because of the formation of shallow marine conditions, subtle changes in the eustatic sea level contributed to the occurrence of several hiatuses (Grant et al., 2017). While these mechanisms are capable of explaining the establishment of the Burdigalian seaway and the formation of distinct sedimentological niches in Switzerland, the drainage reversal during OMM-times possibly requires a change in the tectonic processes at the slab scale. This study thus shows that tectonic and surface signals can be extracted from the stratigraphic record provided that a detailed sedimentological and chronological database is available.

References

Allen, P.A. : Reconstruction of ancient sea conditions with an example from the Swiss Molasse. Marine Geology 60, 455 – 473, 1984.

Allen, P.A., Mange-Rajetky, A. and Matter, A. : Dynamic palaeogeography of the open Burdigalian seaway, Swiss Molasse basin. Eclogae Geologicae Helvetia 78, 351 – 381, 1985.

Allen, P.A. and Allen, J.R. : Basin Analysis: Principles and Applications. Malden, MA. Blackwell Pub., ix, 549 p., ISBN: 0632052074, 2005.

Allen. P. A. and Bass. J. P. : Sedimentology of the Upper Marine Molasse of the Rhône-Alp region. Eastern France: Implications for basin evolution. Eclogae geologicae Helvetia 86(1), 121 – 171, 1993.

Allen, P. A., Crampton, S. L. and Sinclair, H. D. : The inception and early evolution of the North Alpine foreland basin, Switzerland. Basin Research, 3(3),143 – 163, 1991.

Bates, C. C. : Rational theory of delta formation. AAPG Bulletin, 37(9), 2119 – 2162, 1953.

Beaumont, C. : Foreland basins. Geophysical Journal International, 65, (2), 291 – 329, 1981.

Berger, J.-P. : Cartes paléogéographiques-palinspastiques du bassin molassique suisse (Oligocène inférieur – Miocène moyen). N. Jb. Geol. Paläont. Abh. 2002 (1), 1 – 44, 1996.

Bieg, U., Süss, M. P., and Kuhlemann, J. : Simulation of tidal flow and circulation patterns in the Early Miocene (Upper Marine Molasse) of the Alpine foreland basin. Analogue and Numerical Modelling of Sedimentary Systems: From Understanding to Prediction, 40, 145 – 169, 2008.

Boston, K.R., Rubatto, J., Hermann, J., Engi, M. and Amelin, Y. : Geochronology of accessory allanite and monazite in the Barrovian metamorphic sequence of the Central Alps, Switzerland. Lithos, 286 – 287, 502 – 518, 2017.

Burbank, D. W., Engesser, B., Matter, A. and Weidmann, M. : Magnetostratigraphic chronology, mammalian faunas, and stratigraphic evolution of the Lower Freshwater Molasse, Haute-Savoie, France. Eclogae Geologicae Helvetiae, 85(2), 399 – 431, 1992

Cande, S.C. and Kent, D.V. : A new geomagnetic polarity time scale for the Late Cretaceous and Cenozoic. Journal of geophysical research, 97, 913 – 951, 1992.

Cande, S.C. and Kent, D.V. : Revised calibration of the geomagnetic polarity timescale for the Late Cretacesou and Cenocoic. Journal of geophysical research, 100, 6093 – 6095, 1995.

Cederbom, C.E., Sinclair, H.D., Schlunegger, F. and Rahn, M. : Climate-induced rebound and exhumation of the European Alps. Geology, 32, 709 – 712, 2004.

Cederbom, C.E., van der Beek, P., Schlunegger, F., Sinclair, H.D. and Oncken, O. : Rapid extensive erosion of the North Alpine foreland basin at 5-4Ma. Basin Research, 23(5), 528 – 550, 2011.

Davies, J. and von Blanckenburg, F. : Slab breakoff: A model of lithosphere detachment and its test in the magmatism and deformation of collisional orogens. Earth and Planetary Science Letters, 129, 85 – 102, 1995.

DeCelles, P. G. : Late Jurassic to Eocene evolution of the Cordilleran thrust belt and foreland basin system, western USA. American Journal of Science, 304 (2), 105 – 168, 2004.

DeCelles, P.G. and Giles, K.A. : Foreland basin systems: Basin Research 8, 105 – 123, 1996.

Diem, B. : Die Untere Meeresmolasse zwischen der Saane (Westschweiz) und der Ammer (Oberbayern). Eclogae Geologicae Helvetiae, 79 (2), p. 493 – 559, 1986.

Engesser, B. : Die Eomyidae (Rodentia, Mammalia) der Molasse der Schweiz und Savoyens. Systematik und Biostratigraphie. - Schweiz. Paläont. Abh. 112, 1 – 144, 1990.

Fertig, J., Graf, R., Lohr, H., Mau, J., Müller, M. : Seismic sequence and facies analysis of the Puchkirchen Formation, Molasse basin, south-east Bavaria, Germany. Eur. Assoc. Pet. Geosci. Spec. Publ. 1, 277 – 287, 1991.

Flemings, P. B. and Jordan, T. E. : Stratigraphic modeling of foreland basins: Interpreting thrust deformation and lithosphere rheology. Geology, 18 (5), 430 – 434, 1990.

Flemming, B.W. : Geology, Morphology, and Sedimentology of Estuaries and Coasts. Treatise on Estuaries and Coasts, 3 (2), 7 – 38, 2011.

Fry, B., Deschamps, F., Kissling, E., Stehly, L. and Giardini, D. : Layered azimuthal anisotropy of Rayleigh wave phase velocities in the European Alpine lithosphere inferred from ambient noise. Earth and Planetary Science Letters, 297, 95 – 102, 2010.

Füchtbauer, H. : Sedimentpetrographische Untersuchungen in der älteren Molasse nördlich der Alpen. Eclogae Geologicae Helvetia 61, 157 – 298, 1964.

Garefalakis, P. and Schlunegger, F. :. Link between concentrations of sediment flux and deep crustal processes beneath the European Alps. Scientific Reports, 8 (1), 183, 2018.

Haldemann, E. G., Haus, H. A., Holliger, A., Liechti, W., Rutsch, R. F., and Della Valle, G. : Geologischer Atlas der Schweiz, Blatt 1188 Eggiwil (Nr. 75): Schweizerische Geologische Kommission, scale 1:25 000, 1 sheet, 1980.

Handy, M.R., Schmid, S.M., Bousquet, R., Kissling, E. and Bernoulli, D. : Reconciling plate-tectonic reconstructions of Alpine Tethys with the geological – geophysical record of spreading and subduction in the Alps. Earth Science Reviews, 102 (3–4), 121 – 158, 2010.

Handy, M.R., Ustaszewski, K. and Kissling, E. :. Reconstructing the Alps-Carpathians-Dinarides as key to understanding switches in subduction polarity, slab gaps and surface motion. International Journal of Earth Sciences, 104 (1), 1 – 26, 2015.

Herwegh, M., Berger, A., Baumberger, R., Wehrens, P. and Kissling, E. : Large-scale crustal-block-extrusion during Late Alpine collision. Scientific Reports 7, 413, 2017.

Hilgen, F. J., Lourens, L. J., Van Dam, J. A., Beu, A. G., Boyes, A. F., Cooper, R. A., Krijgsman, W., Ogg, J.G., Piller, W.E. and Wilson, D. S. : The Neogene period. In: The geologic time scale, 923 – 978, 2012.

Homewood, P. and Allen, P.A. : Wave-, Tide-, and Current-Controlled Sandbodies in Miocene Molasse, Western Switzerland. The American Association of Petroleum Geologists Bulletin 65, 2534 – 2545, 1981.

Homewood, P., Allen, P.A. and WIlliams, G.D. : Dynamics of the Molasse Basin of western Switzerland. Spec. Publs int. Ass. Sediment., 8, 199 – 217, 1986.

Hurford, A. J. : Cooling and uplift patterns in the Lepontine Alps, south central Switzerland and an age of vertical movement on the Insubric fault line: Contributions to Mineralogy and Petrology, v. 93, 413 – 427, 1986.

Isler, A. and Murer, R. : Geologische Karte der Schweiz, Kartenblatt 1149 Wolhusen 1:25’000, Bundesamt für Landestopographie swisstopo, in press, 2019.

Jordan, T. E. : Thrust loads and foreland basin evolution, Cretaceous, western United States. AAPG bulletin, 65 (12), 2506 – 2520, 1981.

Jordan, T. E. and Flemings, P. B. : Large-scale stratigraphic architecture, eustatic variation, and unsteady tectonism: A theoretical evaluation. Journal of Geophysical Research: Solid Earth, 96 (B4), 6681 – 6699, 1991.

Jost, J., Kempf, O. and Kälin, D. : Stratigraphy and palaeoecology of the Upper Marine Molasse (OMM) of the central Swiss Plateau. Swiss Journal of Geosciences, 109(2), 149 – 69, 2016.

Kälin, D. and Kempf, O. : High-resolution stratigraphy from the continental record of the Middle Miocene Northern Alpine Foreland Basin of Switzerland. N. Jb. Geol. Paläont. Abh., 254, 177 – 235, 2009.

Keller, B. : Fazies und Stratigraphie der Oberen Meeresmolasse (Unteres Miozän) zwischen Napf und Bodensee. Ph.D., Bern, 302 p., 1989.

Keller, B. : Facies of Molasse based on a section across the central part of the Swiss Plateau. Swiss Bull. Angew. Geol., 17/2, 3 – 19, 2012.

Keller, B., Bläsi, H.-R., Platt, N.H., Mozley, P.S. and Matter, A. : Sedimentäre Architektur der distalen Unteren Süsswassermolasse und ihre Beziehung zur Diagenese und den petrophysikal. Eigenschaften am Beispiel der Bohrungen Langenthal. - Nagra Technischer Bericht NTB 90-41, Nagra, Wettingen, 1990.

Kempf, O. Bolliger, T., Kälin, D., Engesser, B and Matter, A. : New magnetostratigraphic calibration of Early to Middle Miocene mammal biozones of the North Alpine foreland basin. Mém. Trav. EPHE Inst. Montpellier 21, 547 – 561, 1997.

Kempf, O. : Magnetostratigraphy and facies evolution of the Lower Freshwater Molasse (USM) of eastern Switzerland. Ph. D., Bern, 138 p., 1998.

Kempf, O. and Matter, A. : Magnetostratigraphy and depositional history of the Upper Freshwater Molasse (OSM) of eastern Switzerland. Eclogae Geologicae Helvetia 92, 97–103, 1999.

Kempf, O., Matter, A., Burbank, D.W. and

Mange, M. : • Depositional and structural evolution of a foreland basin margin in a magnetostratigraphic framework: the eastern Swiss Molasse basin • International Journal of Earth Sciences, 88, 253 – 275, 1999.

Kissling, E. : Deep structure of the Alps—what do we really know? Physics of the Earth and Planetary Interiors, 79 (1-2), 87 – 112, 1993.

Kissling, E., and Schlunegger, F. : Rollback orogeny model for the evolution of the Swiss Alps. Tectonics, 37(4), 1097 – 1115, 2018.

Kuhlemann, J., Frisch, W., Dunkl, I., and Székely, B. : Quantifying tectonic versus erosive denudation by the sediment budget: The Miocene core complexes of the Alps. Tectonophysics, 330(1-2), 1 – 23, 2001.

Kuhlemann, J., Frisch, W., Székely, B., Dunkl, I., and Kázmér, M. : Post-collisional sediment budget history of the Alps: tectonic versus climatic control. International Journal of Earth Sciences, 91(5), 818 – 837, 2002.

Kuhlemann, J. and Kempf, O. : Post-Eocene evolution of the North Alpine Foreland Basin and its response to Alpine tectonics. Sedimentary Geology 152, 45 – 78, 2002.

Kühni, A. and Pfiffner, O. A. : The relief of the Swiss Alps and adjacent areas and its relation to lithology and structure: topographic analysis from a 250-m DEM. Geomorphology, 41(4), 285 – 307, 2001.

Lippitsch, R., Kissling, E. and Ansorge, J. : Upper mantle structure beneath the Alpine orogen from high-resolution teleseismic tomography. Journal of Geophysical Research, 108(B8), 2376, 2003.

Lourens, L. J., F.J. Hilgen, J. Laskar, Shackleton, N. J., and Wilson, D. : The Neogene Period. A Geologic Time Scale 2004, Cambridge University Press, 409 – 440, 2004.

Lu, G., Winkler, W., Rahn, M., von Quadt, A. and Willett, S.D. : Evaluating igneous sources of the Taveyannaz formation in the Central Alps by detrital zircon U–Pb age dating and geochemistry. Swiss Journal of Geosciences, 111(3), 399 – 416, 2018.

Malzer, O., Rögl, F., Seifert, P., Wagner, L., Wessely, G., Brix, F. : Die Molassezone und deren Untergrund. Erdöl und Erdgas in Österreich, 281 – 322, 1993.

Mancktelow, N. : The Simplon Line: a major displacement zone in the western Lepontine Alps. Eclogae Geologicae Helvetiae, 78(1), 73 – 96, 1985.

Mancktelow, N. S., and Grasemann, B. : Time-dependent effects of heat advection and topography on cooling histories during erosion. Tectonophysics, 270 (3-4), 167 – 195, 1997.

Matter, A. : Sedimentologische Untersuchungen im östlichen Napfgebiet (Entlebuch – Tal der Grossen Fontanne, Kt. Luzern). Eclogare Geologicae Helvetia 57, 315 – 429, 1964.

Matter, A., Homewood, P., Caron, C., Rigassi, D., van Stuijvenberg, J., Weidmann, M. and Winkler, W. : Flysch and Molasse of western and central Switzerland. Exc. Guidebook No. 126A 26th Int. Geol. Congr. Schweiz. Geol. Komm. Wepf and Co. Publ., Basel, 1980.

Mazurek M, Hurford A, Leu W. : Unravelling the multi-stage burial history of the Swiss Molasse basin: Integration of Apatite fission track, vitrinite reflectance and biomarker isomerisation analysis. Basin Research, 18, 27 – 50, 2006.

Mein, P. : Résultats du groupe de travail des vertébrés: Biozonation du Néogène méditerranéen à partir des Mammifères. In: Sénès, J. (ed.), Report Report on Activity of the RCMNS Working groups (1971-1975), 78 – 81, Bratislava, 1975.

Mein, P. : Rapport d'activité du Groupe de Travail Vertébrés Mise à jour de la biostratigraphie du Néogène basée sur les Mammifères. Ann. géol. Pays Héilen., Tome hors série, 3, 1367-72. (VII International Congress on Mediterranean Neogene, Athens, 1979), 1979.

Mein, P. : Updating of MN zones. In: Lindsay. E., Fahlbusch, V. and Mein. P. (eds.), European Neogene mammal chronology. NATO ASI, Life Sci. 180, 73 – 90. Plenum Press, New York, 1989.

Miller, K.G., Mountain, G.S., Browning, J.V., Kominz, M., Sugarman, P.J., Christie-Blick, N., Katz, M.E. and Wright, J.D. : Cenozoic global sea level, sequences, and the New Jersey transect: results from coastal plain and conti- nental slope drilling. Rev. Geophys., 36, 569 – 601, 1998.

Miller, K.G., Mountain, G.S., the Leg 150 Shipboard Party, and Members of the New Jersey Coastal Plain Drilling Project : Drilling and dating New Jersey Oligocene–Miocene sequences: Ice volume, global sea level, and Exxon records. Science 271(1), 92 – 94, 1996.

Pippèrr, M. and Reichenbacher, B. : Late Early Miocene palaeoenvironmental changes in the North Alpine Foreland Basin. Palaeogeography, Palaeoclimatology, Palaeoecology 468, 485 – 502, 2017.

Pfiffner, O.A. : Evolution of the north Alpine foreland basin in the Central Alps. Special Publication, International Association of Sedimentologists 8, 219 – 228, 1986.

Pfiffner, O. A., Schlunegger, F. and Buiter, S. J. H. : The Swiss Alps and their peripheral foreland basin: Stratigraphic response to deep crustal processes. Tectonics, 21(2), 2002.

Platt, N. H. and Keller, B. : Distal alluvial deposits in a foreland basin setting—the Lower Freshwater Miocene), Switzerland: sedimentology, architecture and palaeosols. Sedimentology, 39 (4), 545 – 565, 1992.

Reichenbacher, B., Krijgsman, W., Lataster, Y., Pipperr, M., Van Baak, C. G., Chang, L., Kälin, D., Jost, J., Doppler, G., Jung, D., Priet, J., Abdul Aziz, H., Böhme, M., Garnish, J., Kirscher, U. and Bachtadse, V. : A new magnetostratigraphic framework for the Lower Miocene (Burdigalian/Ottnangian, Karpatian) in the North Alpine Foreland Basin. Swiss Journal of Geosciences, 106(2), 309 – 334, 2013.

Sant, K., V. Palcu, D., Mandic, O., and Krijgsman, W. : Changing seas in the Early–Middle Miocene of Central Europe: a Mediterranean approach to Paratethyan stratigraphy. Terra Nova, 29(5), 273 – 281, 2017.

Schaad, W., Keller, B. and Matter, A. : Die Obere Meeresmolasse (OMM) am Pfänder: Beispiel eines Gilbert-Deltakomplexes. Eclogae Geol. Helv., 85, 145 – 168, 1992.

Schlunegger, F., Burbank, D.W., Matter, A., Engesser, B. and Mödden, C. : Magnetostratigraphic calibration of the Oligocene to Middle Miocene (30–15 Ma) mammal biozones and depositional sequences of the Swiss Molasse Basin. Eclogae Geolicae Helvetiae 89, 753 – 788, 1996.

Schlunegger, F., Leu, W. and Matter, A. : Sedimentary Sequences, Seismic Facies, Subsidence Analysis, and Evolution of the Burdigalian Upper Marine Molasse Group, Central Switzerland. The American Association of Petroleum Geologists 81, 1185 – 1207, 1997.

Schlunegger, F. and Willett, S. : Spatial and temporal variations in exhumation of the central Swiss Alps and implications for exhumation mechanisms. Geological Society, London, Special Publications, 154(1), 157 – 179, 1999.

Schlunegger, F. and Hinderer, M. : Crustal uplift in the Alps: why the drainage pattern matters. Terra Nova, 13(6), 425 – 432, 2001.

Schlunegger, F., and Kissling, E. : Slab rollback orogeny in the Alps and evolution of the Swiss Molasse basin. Nature Communications, 6, 8605, 2015.

Schlunegger, F., Anspach, O., Bieri, B., Böning, P., Kaufmann, Y., Lahl, K., Lonschinski, M., Mollet, H., Sachse, D., Schubert, C., Stöckli, G. and Zander, I. : Geologische Karte der Schweiz, Kartenblatt 1169 Schüpfheim 1:25’000, Bundesamt für Landestopographie swisstopo, 2016.

Short, A. D. : Coastal Processes and Beaches. Nature Education Knowledge 3(10): 15, 2012.

Sinclair, H.D., Coakley, B.J., Allen, P.A. and Watts, A.B. : Simulation of foreland basin stratigraphy using a diffusion model of mountain belt uplift and erosion: An example from the Central Alps, Switzerland. Tectonics 10, 599 – 620, 1991.

Sinclair, H.D. and Allen, P.A. : Vertical versus horizontal motions in the Alpine orogenic wedge: stratigraphic response in the foreland basin. Basin Research 4, 215 – 232, 1992.

Spicher, A. : Geologische Karte der Schweiz, 1, 500,000. Schweiz. Geol. Komm., Basel, 1980.

Strunck, P. and Matter, A. : Depositional evolution of the western Swiss Molasse. Eclogae Geologicae Helvetiae, 95, 197 – 222, 2002.

Ustaszewski, K., Schmid, S.M, Fügenschuh, B., Tischler, M., Kissling, E. and Spakman, W. : A map-view restoration of the Alpine-Carpathian-Dinaridic system for the Early Miocene. Swiss Journal of Geosciences, 101 (SUPPL. 1), 273 – 294, 2008.

Wanner, J., Gisler, C., Jost, J., Christener, F. Ninck, T. : Geologische Karte der Schweiz, Kartenblatt 1148 Sumiswald 1:25'000, Bundesamt für Landestopographie swisstopo, in press, 2019.

Wehrens, P. : Structural evolution in the Aar Massif (HaslitaI transect): Implications for midcrustal deformation. Ph.D., Bern, 2015.

Wehrens, P., Baumberger, R., Berger, A. and Herwegh, M. : How is strain localized in a meta-granitoid, mid-crustal basement section? Spatial distribution of deformation in the central Aar massif (Switzerland), Journal of Structural Geology, 94, 47 – 67, 2017.

Willett, S. D. : Late Neogene erosion of the Alps: A climate driver?. Annual Review of Earth and Planetary Sciences, 38, 411-437, 2010.

Zachos, J., Pagani, M., Sloan, L. Thomas, E. and Billups, K. : Trends, rhythms and aberrations in global climate 65 Ma to present, Science, 292, 686 – 693, 2001.

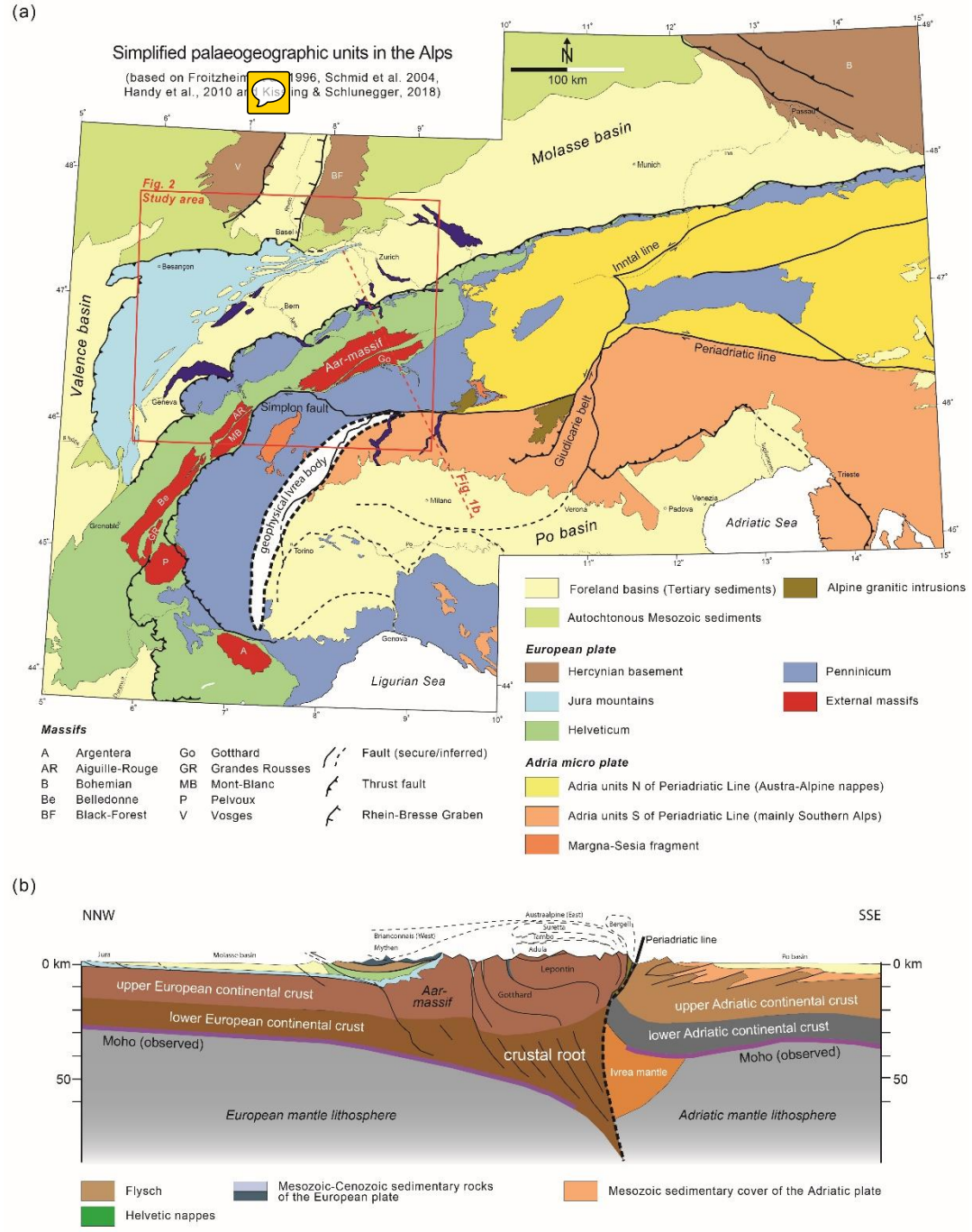

Figure 1: a) Simplified geological map of the European Alps. It is based on the compilation by Kissling and Schlunegger (2018) was updated by using additional information published in Handy et al. (2015) and in Pippèrr and Reichenbacher (2017).

b) Simplified geological-geophysical section through the central European Alps, taken and modified from Kissling and Schlunegger (2018).

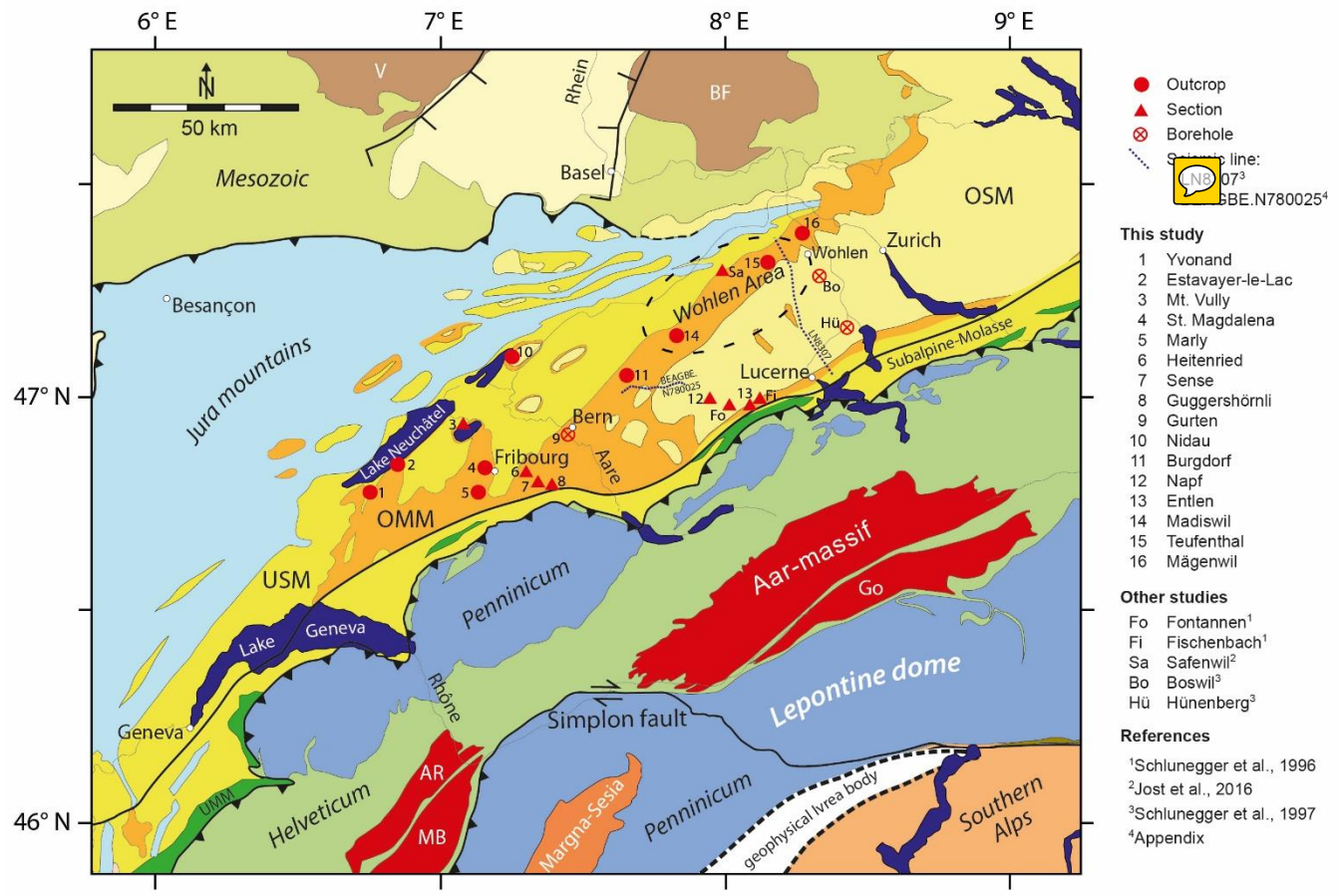

Figure 2: Simplified geological-geophysical section through the central European Alps, taken and modified from Kissling and Schlunegger (2018).

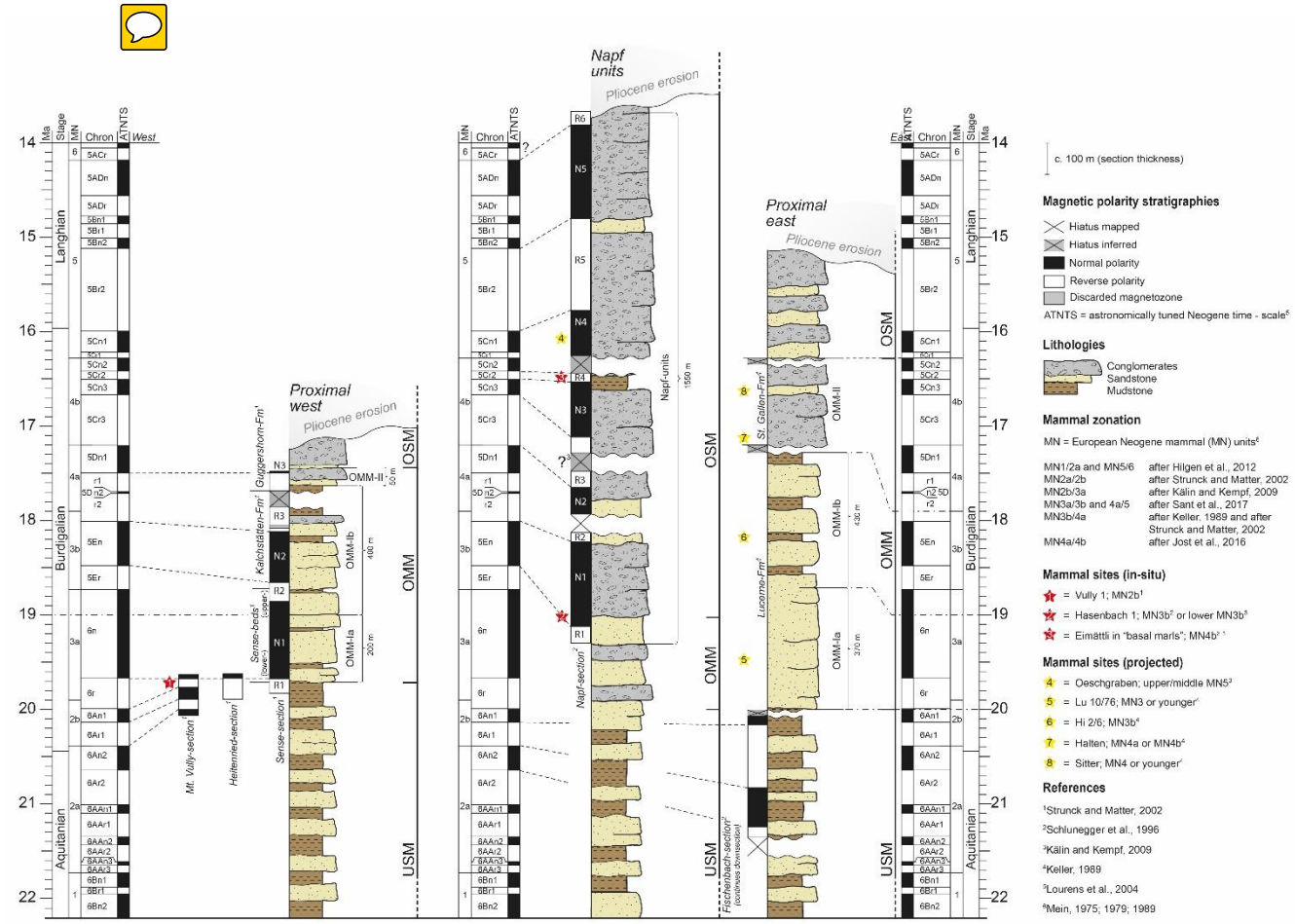

Figure 3: Composite stratigraphies illustrating the sedimentary architecture at the proximal basin border in the western Molasse basin (proximal west) in the central part of the Molasse basin (Napf units) and in the eastern basin (proximal east). A composite section for the proximal west has been drawn based on data from the Mt. Vully- and Heitenried-sections, drillings, and from surface information from the Sense-section (Sense beds and Kalchstätten-Fm) (Strunck and Matter, 2002). The composite section representative for the sequence at the Napf is mainly based on the sedimentary log by Schlunegger et al. (1996; see their Schwändigraben- and Fontannen-sections) complemented with information from the geological map of the region (Schlunegger et al., 2016). Please note that Kälin and Kempf (2009) proposed the occurrence of a very short hiatus recorded by magnetozone R3 within the Napf-units which we do not discuss in detail for simplicity purposes. The composite section illustrating the situation at the proximal basin border east of the Napf represents the sedimentary architecture as far east as of Lake Zurich (Fig. 2). It is based on data from Keller (1989, see his Rümlig-, Ränggloch- and Lucerne-sections) and data from Schlunegger et al., (1996, see their Fischenbach-section) and geological maps of the region (Wolhusen; Isler and Murer, 2019). Please note that the Entlen-section is situated immediately east of the Napf (Fig. 4a) where the basal part (Lucerne-Fm) can be characterized by the composite section of the proximal east, while the topmost part is made up of the conglomerates of the Napf-units. Detailed sedimentological data of the Sense-beds and the Lucerne-Fm can be found in Fig. 5. Note, that the Molasse units written in capitals (i.e. USM, OMM and OSM) are based on the lithological architecture and thus on the facies associations identified in the field.

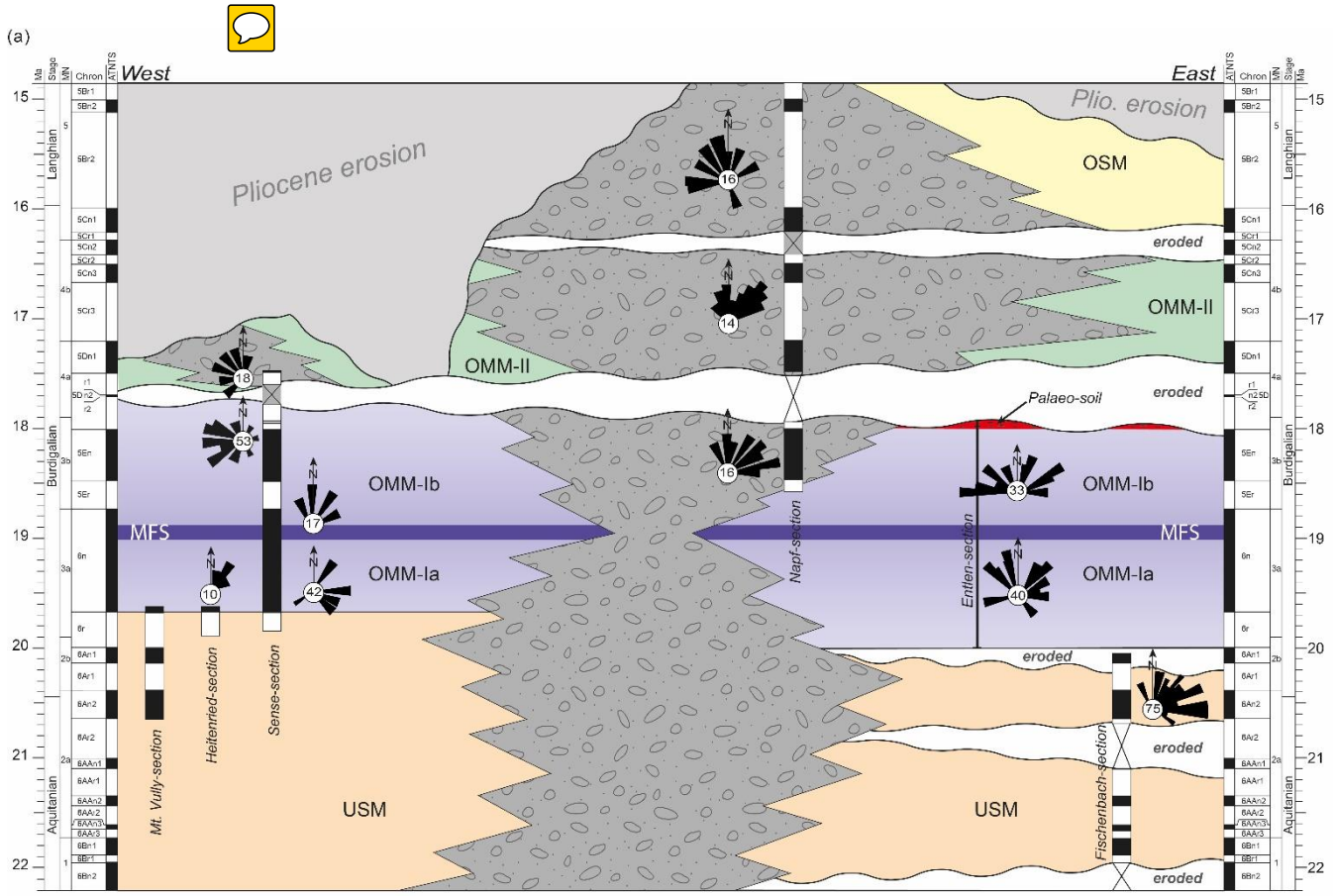

Figure 4: a) Chronological (Wheeler) diagram of the Molasse deposit at the proximal basin border between Fribourg and Lucerne (Fig. 2). The following magnetostratigraphic data has been used: Mt. Vully, Heitenried and Sense (Strunck and Matter, 2002), and Napf and Fischenbach (Schlunegger et al., 1996). Palaeo-discharge directions from Heitenried and the upper part of the Sense-section are taken from Strunck and Matter (2002). Note, that the Entlen-section is not calibrated with magnetostratigraphic data but has been adjusted using regional information (see text for further details and Fig. 3 for synthetic sections of the region). MFS = Maximum flooding stage. Note that the Pliocene phase of erosion removed most of the OMM II records in western Switzerland. We infer marine conditions in the western Swiss Molasse basin during OMM II times because (i) marine conditions were present east of the Napf-units, and (ii) material transport occurred towards the west, which implies that marine conditions were also present west of the Napf megafan at that time, as confirmed by mapping (e.g., Wanner et al., 2019).

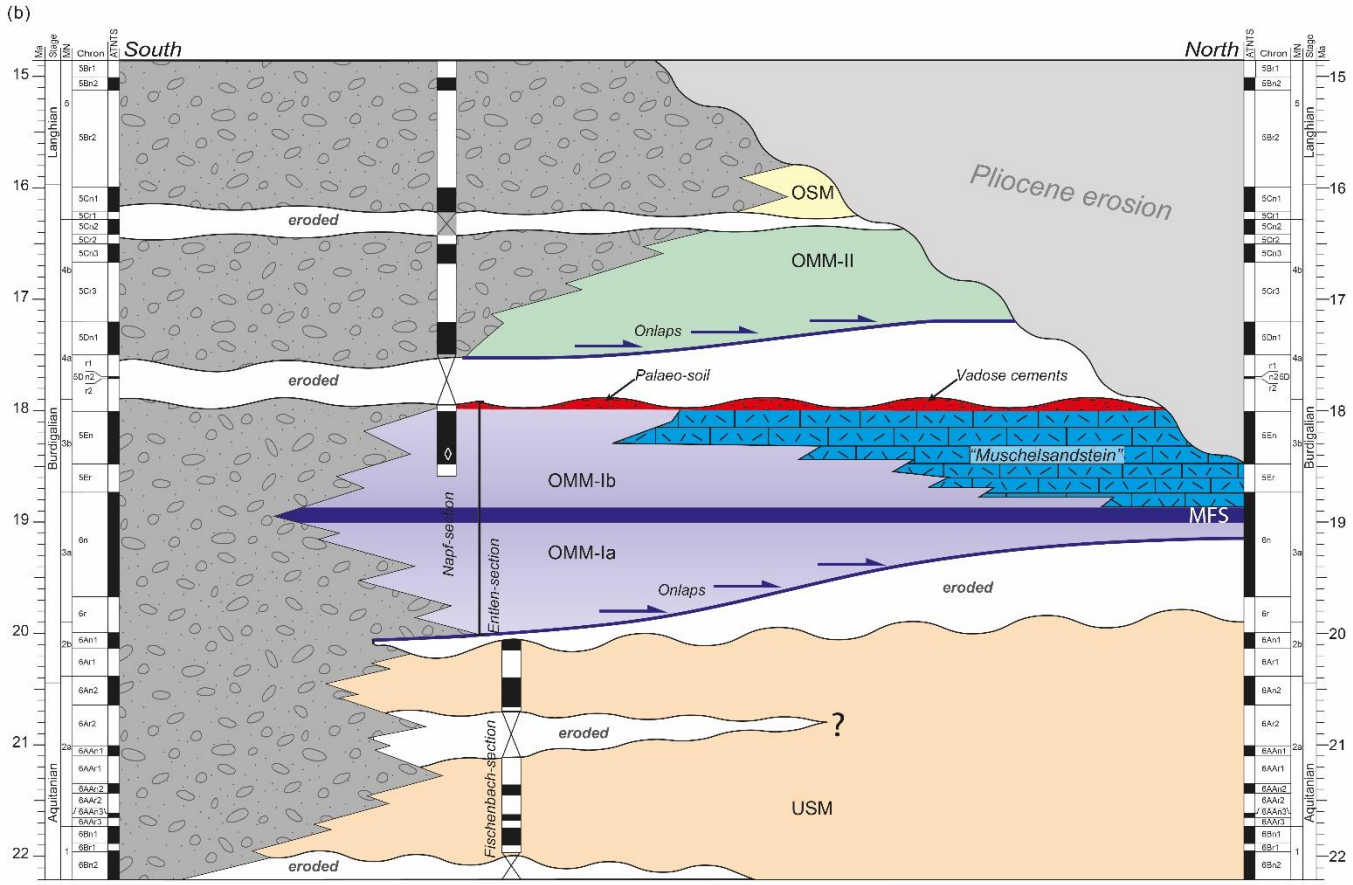

b) Chronological (Wheeler) diagram of the Molasse sequence across the basin within a section between Entlen (site 13) and Madiswil (site 14, both on Fig. 2). See text for further details. The onlaps (blue arrows) are based on interpretations from seismostratigraphic data (Schlunegger et al., 1997). MFS = Maximum flooding stage.

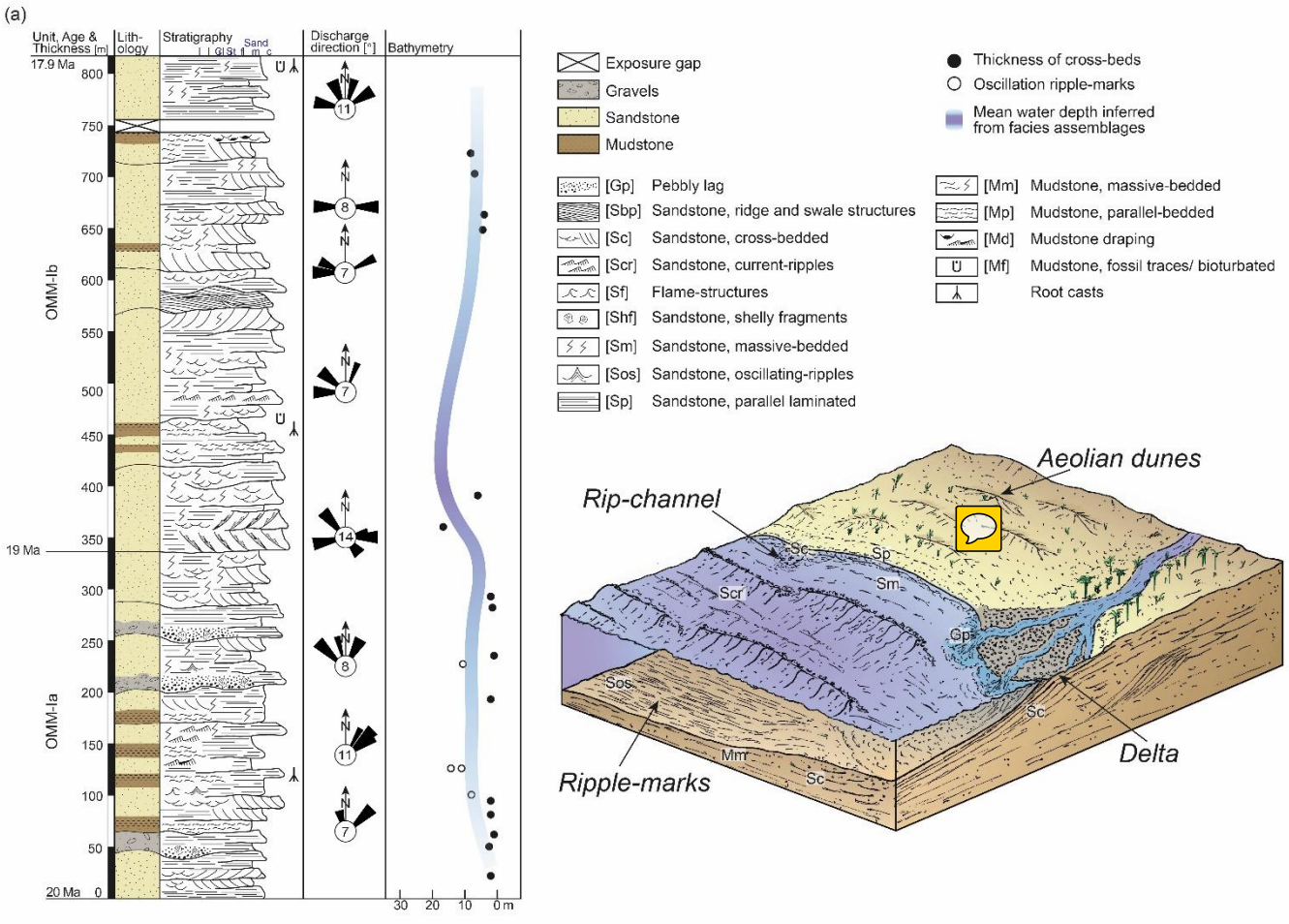
(a)
Unit, Age & Thickness [m]
Lith-ology
Stratigraphy
Sand
Discharge direction [°]
Bathymetry
17.9 Ma
19 Ma
20 Ma
OMM-Ib
OMM-Ia
800
750
700
650
600
550
500
450
400
350
300
250
200
150
100
50
0
30 20 10 0 m
Exposure gap
Gravels
Sandstone
Mudstone
Thickness of cross-beds
Oscillation ripple-marks
Mean water depth inferred from facies assemblages
[Gp] Pebbly lag
[Sbp] Sandstone, ridge and swale structures
[Sc] Sandstone, cross-bedded
[Scr] Sandstone, current-ripples
[Sf] Flame-structures
[Shf] Sandstone, shelly fragments
[Sm] Sandstone, massive-bedded
[Sos] Sandstone, oscillating-ripples
[Sp] Sandstone, parallel laminated
[Mm] Mudstone, massive-bedded
[Mp] Mudstone, parallel-bedded
[Md] Mudstone draping
[Mf] Mudstone, fossil traces/ bioturbated
Root casts
Aeolian dunes
Rip-channel
Sc
Sp
Sm
Scr
Gp
Sos
Sc
Mm
Sc
Ripple-marks
Delta

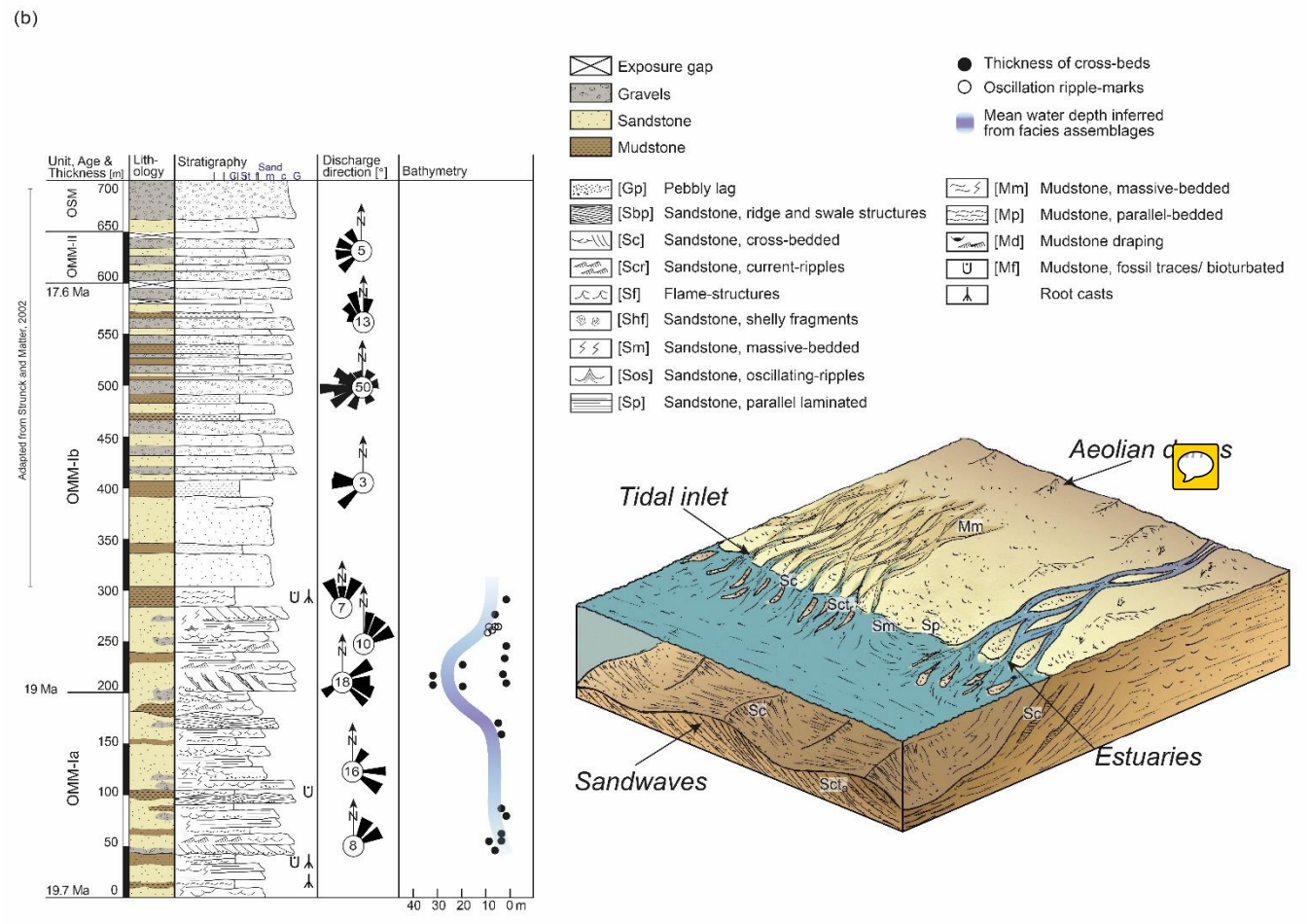

Figure 5 (a and b): Sedimentological log of the a) Entlen- and b) Sense-section. See Fig. 2 for location of sections, Fig. 4 for chronological framework of the deposits and Table 1 (Appendix) for further sedimentological details and abbreviations of the lithofacies. The block-diagrams illustrate the palaeo-geographical conditions from a conceptual point of view. Please note that the palaeo-bathymetry values are minimum estimates, and that the mean water depths have been inferred from the assignments of the lithofacies to the depositional environment. This might explain why the numerical values for water-depths based on cross-bed thicknesses and our inferred mean water-depth estimates deviate, in particular between c. 200 m and 250 m of the Sense-section.

(a)

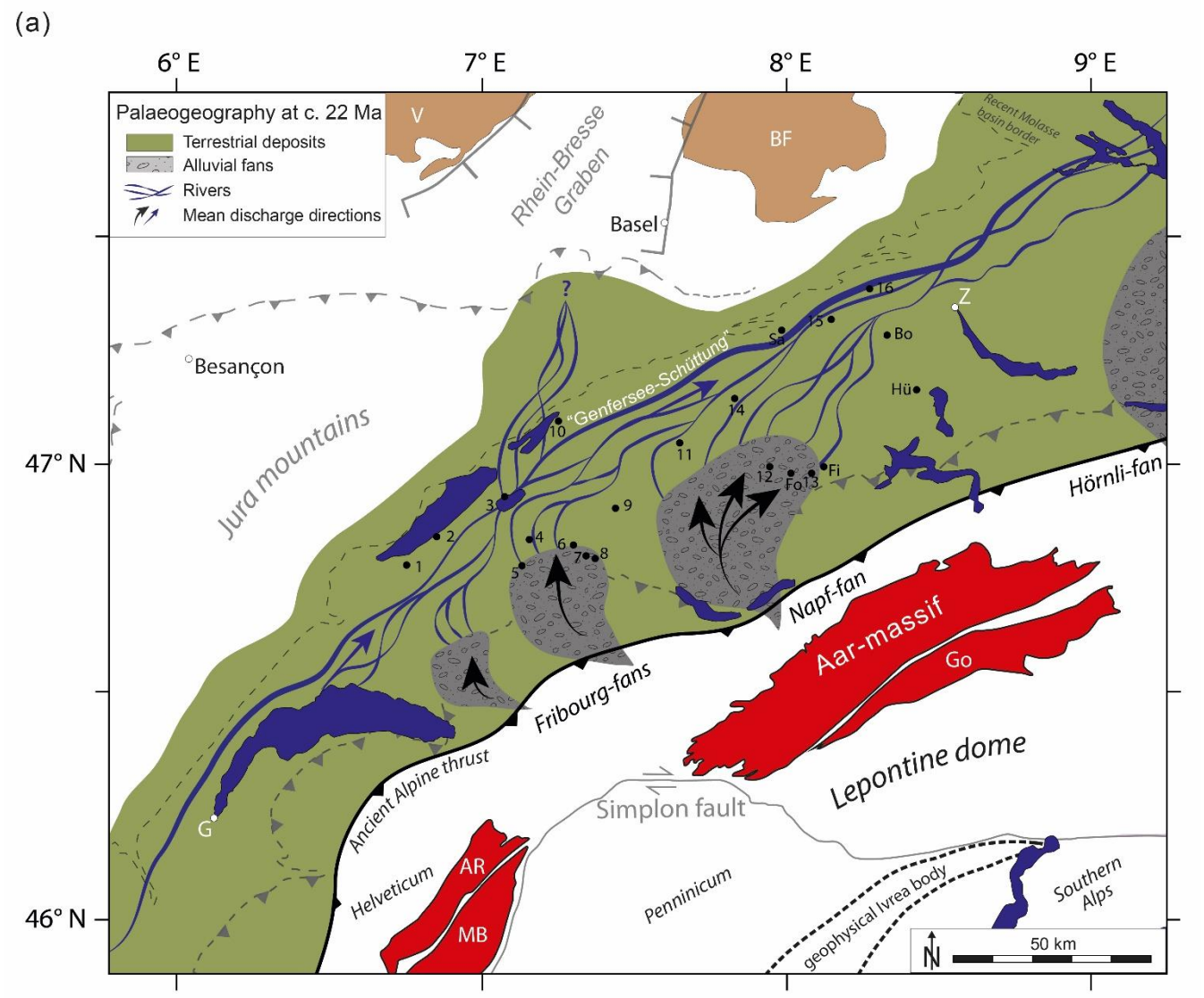
Palaeogeography at c. 22 Ma
Terrestrial deposits
Alluvial fans
Rivers
Mean discharge directions
6° E
7° E
8° E
9° E
47° N
46° N
V
BF
Rhein-Bresse Graben
Basel
Recent Molasse basin border
Besançon
Jura mountains
"Genfersee-Schüttung"
Z
Bo
Hü
Fi
Fo
Hörnli-fan
Napf-fan
Aar-massif
Go
Fribourg-fans
Lepontine dome
Ancient Alpine thrust
Simplon fault
Helveticum
AR
MB
Penninicum
geophysical Ivrea body
Southern Alps
G
N
50 km

(b)

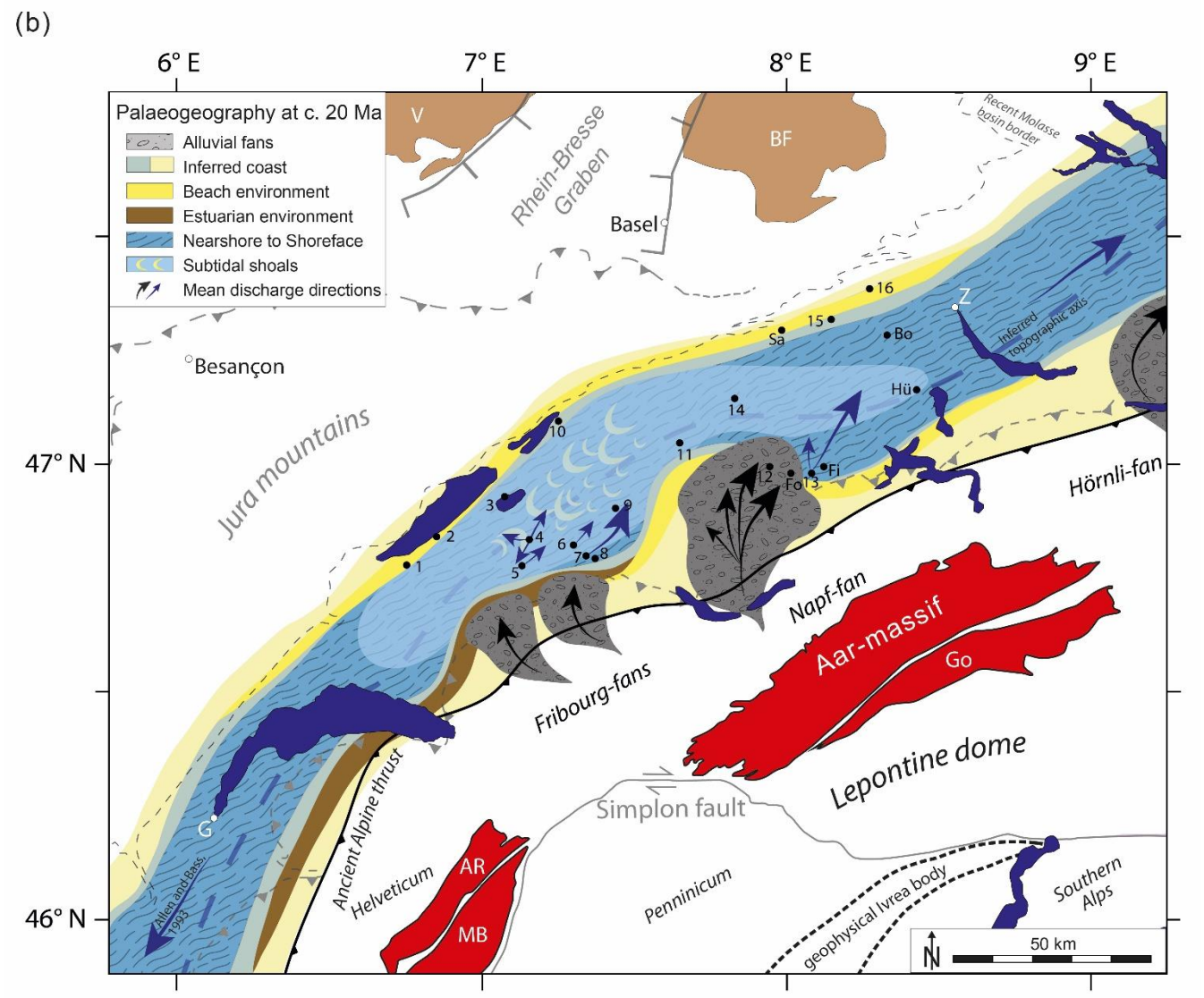
6° E
7° E
8° E
9° E
47° N
46° N
Palaeogeography at c. 20 Ma
Alluvial fans
Inferred coast
Beach environment
Estuarian environment
Nearshore to Shoreface
Subtidal shoals
Mean discharge directions
V
BF
Rhein-Bresse Graben
Basel
Recent Molasse basin border
Besançon
Jura mountains
Inferred topographic axis
Hörnli-fan
Napf-fan
Aar-massif
Go
Fribourg-fans
Lepontine dome
Simplon fault
Ancient Alpine thrust
Helveticum
AR
MB
Penninicum
geophysical Ivrea body
Southern Alps
Allen and Bass, 1993
Sa
Bo
Hü
Fo
Fi
Z
G
1
2
3
4
5
6
7
8
9
10
11
12
13
14
15
16
N
50 km

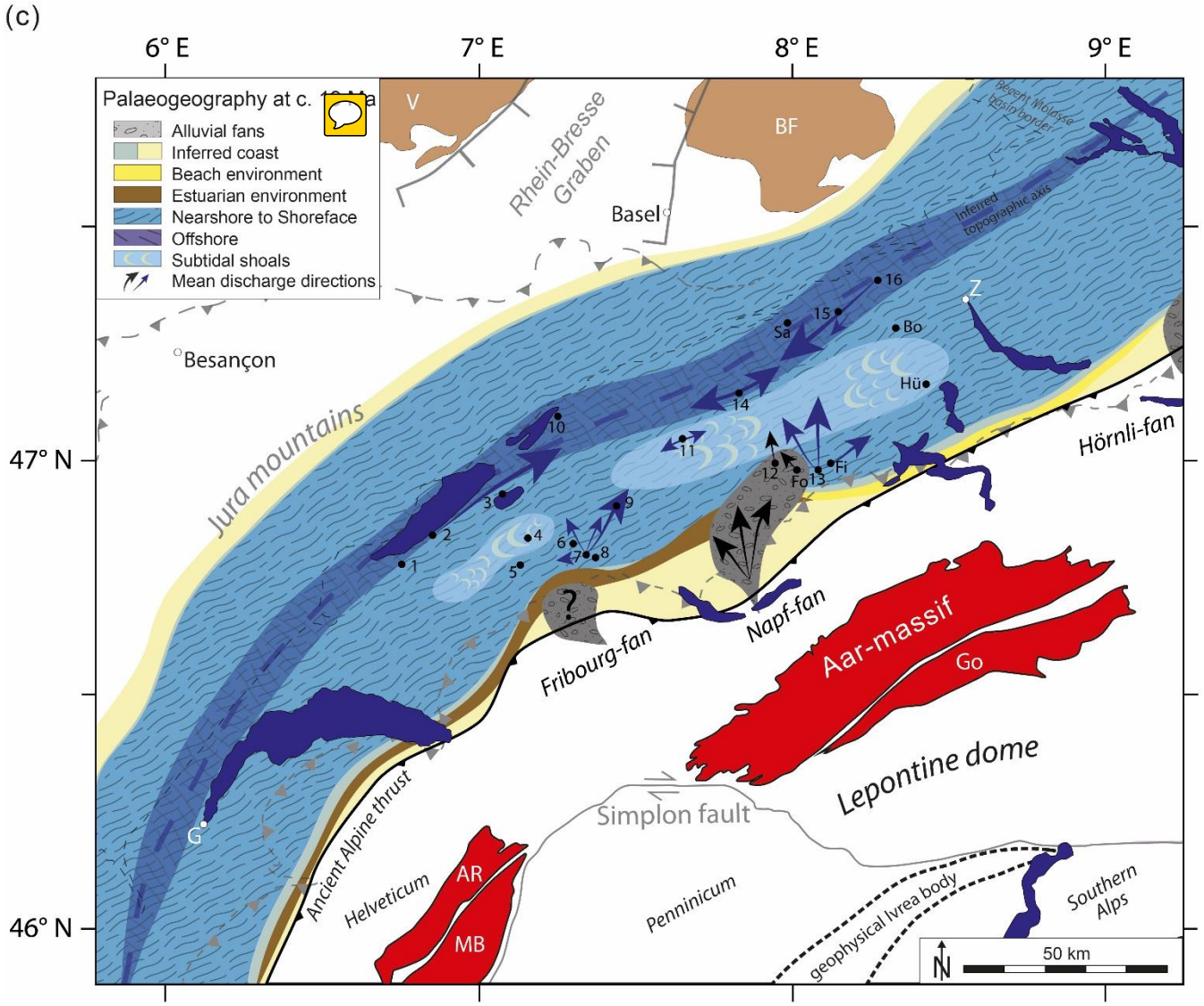
(c)
6° E
7° E
8° E
9° E
47° N
46° N
Palaeogeography at c.
Alluvial fans
Inferred coast
Beach environment
Estuarian environment
Nearshore to Shoreface
Offshore
Subtidal shoals
Mean discharge directions
V
BF
Rhein-Bresse Graben
Basel
Besançon
Jura mountains
Hörnli-fan
Napf-fan
Fribourg-fan
Aar-massif
Go
Lepontine dome
Simplon fault
Ancient Alpine thrust
Helveticum
AR
MB
Penninicum
geophysical Ivrea body
Southern Alps
G
Sa
Bo
Hü
Z
Fo
Fi
50 km
N

5

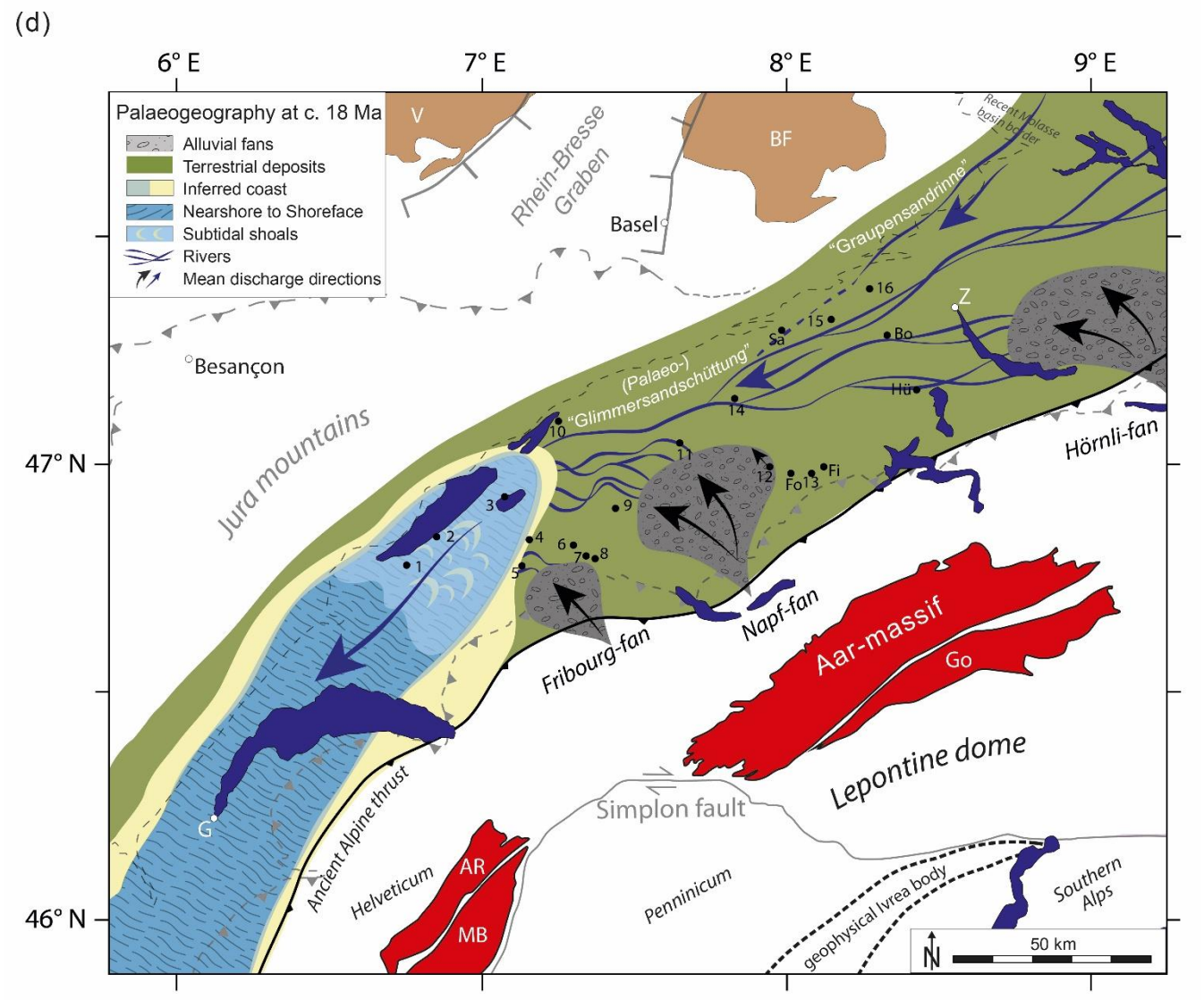

Figure 6 (a to d): Palaeo-geographical situation of the Molasse basin at a) c. 22 Ma, b) c. 20 Ma, c) c. 19 Ma and d) c. 18 Ma modified after Kuhlemann and Kempf (2002). Please note that all maps also show the present-day lithotectonic units within the Alps and the Jura mountains for orientation purposes (dashed lines and grey coloured lines). We acknowledge, that the position of these and the surface patterns (such as lakes) were certainly different during deposition of the Molasse deposits. The location of the palaeo-thrust fronts (thick line) have been adapted from Kuhlemann and Kempf (2002). Black dots mark study sites for orientation purposes. Please refer to Fig. 1 for the complete legend.

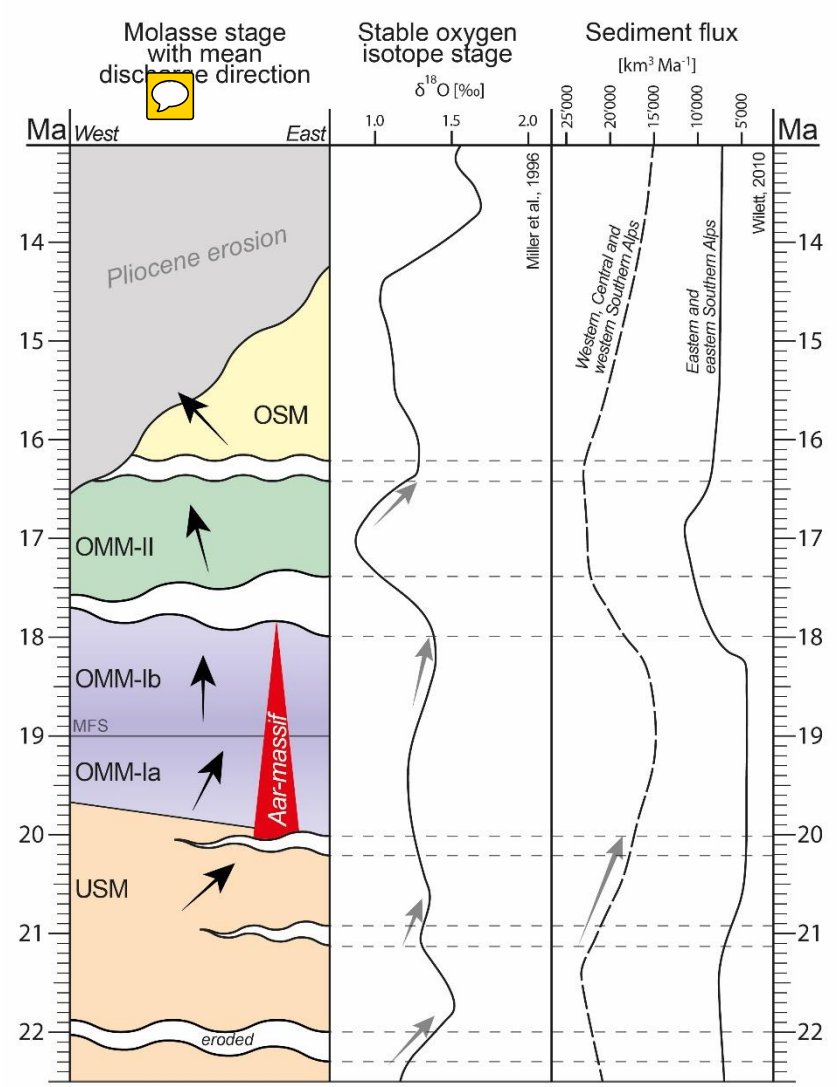

Figure 7: Molasse stages with mean discharge directions with hiatus plotted against stable oxygen isotope stages (Miller et al., 1996) and sediment flux (Willet, 2010). Red triangle marks the onset of delamination and fast exhumation of the Aar-massif (Herwegh et al., 2017). Grey arrows mark drops in sea level and sediment flux possibly contributing to the related hiatus. MFS = Maximum flooding stage.